LAJSBA
LATIN AMERICAN JOURNAL OF SEDIMENTOLOGY AND BASIN ANALYSIS | VOLUME 31 (2) 2024, 162-187

DECIPHERING THE ORIGIN OF LINEAR LANDFORMS USING DIFFERENT SEDIMENTOLOGICAL TOOLS IN THE FIAMBALÁ VALLEY (CATAMARCA)

Delfina Fernandez Molina[1,2], Patricia L. Ciccioli[1,2], Leopoldo D. Serpa[1,3], Paloma Amado Silvero[1,2]*

[1]Universidad de Buenos Aires. Facultad de Ciencias Exactas y Naturales, Departamento de Ciencias Geológicas. Buenos Aires, Argentina.
[2]CONICET - Universidad de Buenos Aires. Facultad de Ciencias Exactas y Naturales. Instituto de Geociencias Básicas, Aplicadas y Ambientales de Buenos Aires (IGeBA). Buenos Aires, Argentina.
[3]Universidad Nacional de la Patagonia Austral (UNPA). Unidad Académica Río Turbio (UART). Instituto de Ciencias del Ambiente, Sustentabilidad y Recursos Naturales (ICASUR). Av. de los Mineros 1260. Río Turbio (CP 9407), Santa Cruz.
*Corresponding author: delfina.f.m@gmail.com

ARTICLE INFO

Article history
Received January 10, 2024
Accepted December 4, 2024
Available online December 12, 2024

Handling Editor
M. Sol Raigemborn

Keywords
Linear morphologies
Sandy gravel
Desert pavement
Intermountain valley
Apocango River

ABSTRACT

The current study is centered on the morphological, textural, and compositional characterization of several linear landforms identified in the west and center of the Fiambalá Valley, in the western region of the Catamarca province (Argentina), along the terraces of the Apocango River. These landforms are slightly asymmetric to symmetric, with rounded crests, a few meters high (between 0.3 and 3.5 m) and several meters wide (from 8 to 14.5 m). They have straight to slightly sinuous ridges with NE-E to SW-W direction and are arranged as isolated bodies. The superficial cover has a bimodal frequency distribution with a primary mode in medium to coarse pebble (-4.5 to -3.5 φ) and a secondary mode in fine sand (2.5 φ). Gravel clasts are sub-rounded, with moderate sphericity, and predominantly compact-elongated shape. The analysis of high-resolution photographs of the superficial cover showed they present an open to moderate packing (44.49 - 58.60% of clasts). In a cross-sectional profile, it was observed that internally they consist of fine to medium sand (x: 2.66 - 1.31 φ). Gravel composition is made primarily by clasts of green sedimentary lithics (22.92 - 32.72%), followed by acidic volcanic lithics (15 - 21.49%), purple sedimentary lithics (13.72 - 17.04%), and basic (10.60 - 17.78%) and intermediate (9.74 - 12.93%) volcanic lithics, thus classified as lithic gravels. The sandy fraction is composed of lithics (35.71 - 47.51%), followed by quartz (23.59 - 37.92%), and feldspars (19.80 - 32.76%); consequently, classified as feldspathic litharenites. Regarding the lithic fragments, volcanic types predominate (27.41 - 37.70%), being those of acidic composition with felsitic and microgranular paste (20.06 - 31.15%) the most represented. The thicker superficial cover with open to moderate packing is interpreted as poorly evolved desert pavement. Deposit composition suggests that the main contribution of the gravelly and sandy material comes from the west (Sistema de Famatina), congruent with the source area of the Apocango alluvial system and the preferential directions of wind that transports material from the SW-WSW towards NNE-NE. The rounded crest, straight to slightly sinuous ridges, and their parallel orientation to the main drift potential direction (RDD) agree with the characteristics of moderately to highly deflated linear dunes. Regarding their origin, initially, the area was dominated by eolian sedimentation of linear dunes associated with the migration of wind ripples. In a second stage deflation prevailed, preserving only fine sediments in sheltered areas,

probably related to the margins of small secondary channels or gullies. In this stage, active deflation altered the original linear dune morphology and gave rise to poorly evolved desert pavements. This process stabilized linear dunes, forming a protective layer and ensuring immobility.

INTRODUCTION

The Fiambalá Basin is an intermontane valley located in the western sector of the Catamarca province, northwest of Argentina, where arid climatic conditions prevail. Within this context, eolian processes constitute one of the primary shaping agents of the landscape. In the central and eastern parts of the valley, accumulations of eolian sands form the Medanitos-Saujil and Tatón dune fields, respectively (Fig. 1). However, in the western sector of the valley, eolian accumulations are scarce and isolated, such as in the Campo de Anchoco (Fig. 1). In contrast, erosive eolian processes (deflation) prevail in the rest of the area.

Eolian bedforms can be described based on field and aerial photograph measurements according to Wilson's (1972) proposal, which categorizes them into three main types: ripples, dunes, and draas. Ripples have crest lines oriented transversely to the direction of the wind, with heights ranging from millimeters to a few meters (Bagnold, 1954; Wilson, 1972). Depending on their grain size, they can be characterized as sand ripples (Bagnold, 1954; Sharp, 1963) and granule ripples (Sharp, 1963; Fryberger *et al.*, 1992), or, as some authors suggest, megaripples (Taira *et al.*, 1979; Greeley and Iversen, 1985; De Silva *et al.*, 2013; Gough *et al.*, 2020). Dunes can be defined simply as a hill or ridge of sand piled up by the wind (Pye and Tsoar, 2009), they vary in height from 0.1 to 100 m and exhibit a wide range of morphological forms. They can be classified based on their shape, position, and number of slipfaces they possess (McKee, 1979) recognizing barchans, transverse (barchanoids) ridges, linear dunes, domes, and stars. For example, simple linear dunes are narrow dune ridges with straight to sinuous crest lines which may be rounded to sharp in cross-section (Pye and Tsoar, 2009). They are commonly identified by their straightness and parallelism (Lancaster, 1995). Draas are the largest sand bedforms, ranging from 20 to 450 m in height, characterized by the superimposition of smaller dunes (Havholm and Kocurek,1988).

In this contribution, we present the recognition and morphological, textural, and compositional characterization of certain linear sandy gravel landforms. These linear morphologies, a few meters high and several meters wide, are developed in the western and middle areas of the valley on the terraces of the Apocango River (Fig. 1). Finally, based on the description provided herein and its comparison with those recorded in the literature, it is possible to define their origin concerning different factors, such as climate and provenance of the deposits, which are discussed in this work. For this purpose, the climatic characteristics of the area are also presented and considered, emphasizing the directions and maximum wind velocities recorded by an *in situ* meteorological station. Additionally, a drift potential analysis was conducted to describe the sand activity in relation to the wind power in the studied area.

GEOLOGICAL AND GEOMORPHIC SETTING

Geological context

The study area is located in the Central Andes of Argentina and corresponds to the northern sector of the subhorizontal subduction segment of the Nazca oceanic plate (27º - 33º30'S), corresponding to the Cordillera Frontal - Precordillera - Sierras Pampeanas - Sistema de Famatina (Ramos, 1999; Ramos *et al.*, 2002). The region is characterized by a relief composed of mountain ranges oriented generally north-south, separated by intermontane valleys, among which is the Fiambalá Valley (Fig. 1a). This valley aligns with a transitional zone between the Northwestern Sierras Pampeanas to the east and north, represented by the Sierra de Fiambalá and the Cordillera de San Buenaventura, respectively; the Sierra de Las Planchadas and Narváez, belonging to Sistema de Famatina, to the west; and the Puna Austral further north (Fig. 1a). The area of interest for this work is in the western and central parts of the valley in a narrow gorge delimited by Pliocene-Pleistocene pedimented unit (Rodados de la Puna

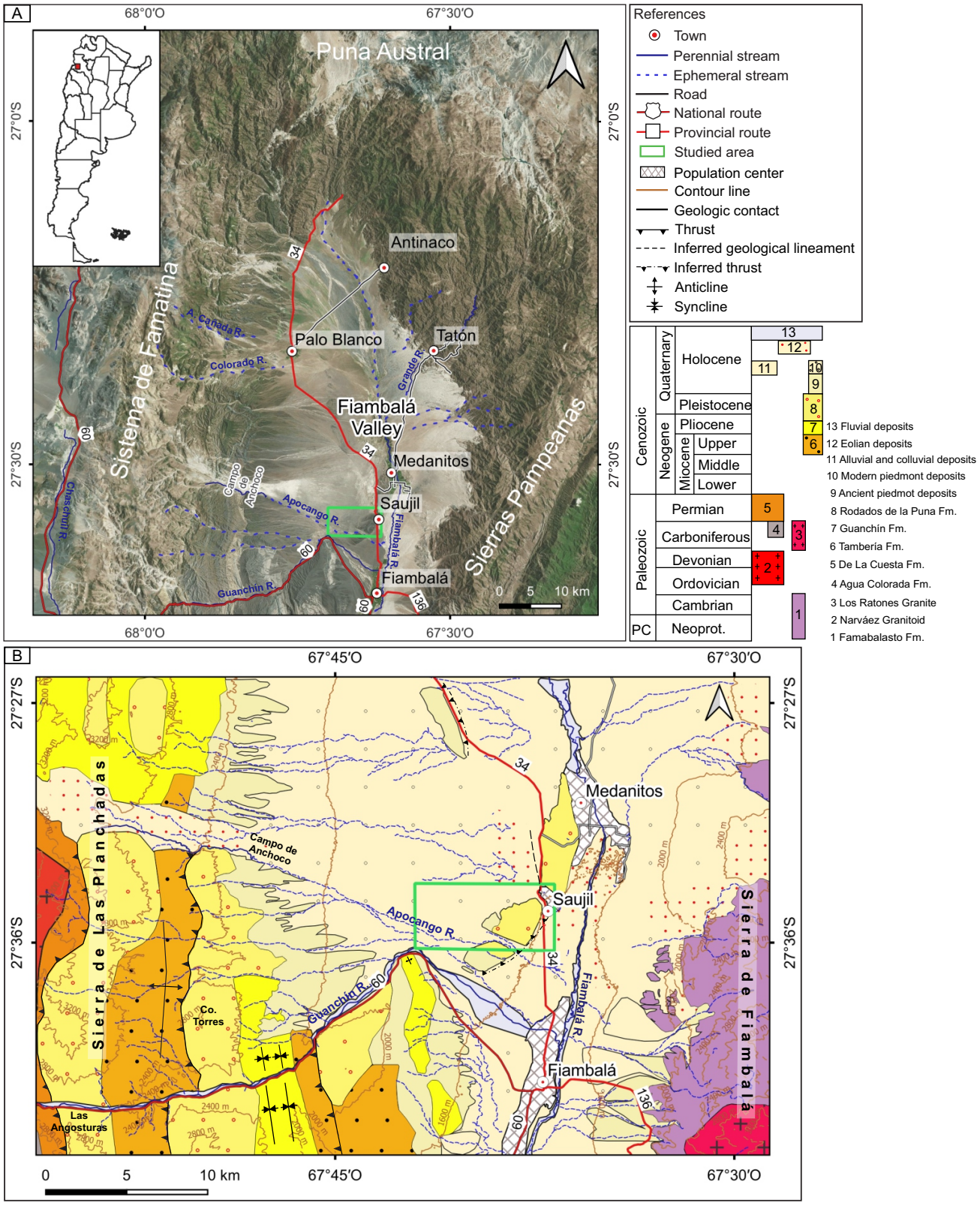

Figure 1. a) General location map of the Fiambalá Valley with the main morphostructural units that delimit it and the detailed studied area. The red square represents the studied area on the map of Argentina. **b)** Geological map of the area and stratigraphic chart based on and modified from Rubiolo *et al.* (2003).

Formation) and ancient piedmont deposit levels, on the Apocango River terraces. It extends between the geographic coordinates of 27°34'45.84" and 27°36'53.97"S and 67°41'28" and 67°36'57.74"W, in the Tinogasta Department, west of the Catamarca province, NW of Argentina (Fig. 1a).

The Fiambalá Valley is segmented by basement blocks bounded by high-angle reverse faults (Sierras de Fiambalá, Las Planchadas and Narváez, and the Cordillera de San Buenaventura, Ramos *et al.*, 2002; Quiroga *et al.*, 2021; Fig. 1b). The Sierras Pampeanas, represented in the eastern and northern sectors of the area, consist of tilted blocks of medium-grade metamorphic rocks transitioning to high-grade rocks of Neoproterozoic-Cambrian age (Famabalasto Formation) and Carboniferous granites (Los Ratones Granite; Rubiolo *et al.*, 2003). In the western sector, in Sierra de Las Planchadas and Narváez (Fig. 1b), the Las Planchadas Formation outcrops, composed of Ordovician acidic to basic sedimentary and volcanic rocks, and Ordovician-Devonian granitic bodies (Narváez Granitoid; Rubiolo *et al.*, 2003). Additionally, Carboniferous green sedimentary rocks (Agua Colorada Formation) and Permian red sandstones (De La Cuesta Formation) occur. Above them, a Cenozoic continental succession is recognized, represented by the Tambería, Guanchín, and Rodados de la Puna formations. The Tambería Formation consists of reddish-brown sandstones, brown and greenish-gray mudstones, gray conglomerates, and sparse tuffaceous levels (Deri *et al.*, 2019). The Guanchín Formation is composed of yellowish-gray sandstones with abundant pyroclastic material and intercalations of polymictic conglomerates and mudstones. Finally, the Rodados de la Puna Formation is dominated by polymictic conglomerates (Fig. 1b). To the north, the Cordillera de San Buenaventura, with an approximately east-west orientation, separates the valley from the Puna Austral. This region, between the Upper Miocene and Holocene, experienced intense acidic to intermediate volcanism, exemplified by the Aguada Alumbrera Ignimbrites and the Cerro Blanco Volcanic Complex (Montero López *et al.*, 2010, 2011). The latter is part of a collapsed caldera system associated with pyroclastic deposits and acidic lavas (Báez *et al.*, 2017).

Geomorphological context

The Fiambalá Valley is characterized by significant sandy eolian deposits, mainly in the central and eastern parts, and by fluvial-alluvial deposits. The Apocango River is one of the tributaries of the Fiambalá River, with ephemeral braided character shaping a gravel sandy alluvial plain. It has a transverse disposition to the Sierra de Las Planchadas (Fig. 1b), draining the western sector of the region and transporting sediments towards the center of the Fiambalá Valley. There, it flows into the homonymous river, forming a terminal fan with a distributary design covering an area of 1.37 km^2 (Fig. 2). Due to fluvial activity, mass wasting processes, and weathering of Pliocene-Pleistocene units (such as the Rodados de la Puna Formation), pediments are developed (Fig. 2, Rubiolo *et al.*, 2003). Additionally, at least two piedmont deposit levels are recorded in the area, one probably of Pleistocene age (ancient piedmont deposits) and the other Holocene (modern piedmont deposits). Both pediments and piedmont deposit levels are affected by neotectonics, recognized by hills that can be seen to the south and north of the town of Saujil, as well as further north in the valley towards the town of Palo Blanco (Fig. 1; Rubiolo *et al.*, 2003; Ratto *et al.*, 2013).

Regarding the fluvial system of the Apocango River, in the study area, it is characterized by sandy gravel deposits deposited by upper regime fluid flows, with alternation of non-cohesive hyper-concentrated flows and thin eolian-fluvial interaction deposits generated by the migration of wind ripples over exposed river bars in the alluvial plain (Fernandez Molina, 2020; Ciccioli *et al.*, 2021). Active and semi-active to inactive eolian field geomorphic units develop to the south and west of the localities of Medanitos and Saujil (Fig. 2). In the active eolian field unit, three subenvironments are recognized: 1) an eolian dune field where barchanoid-ridges and barchan dunes migrate; 2) a sand sheet dominated by deflation areas, sand shadows, zibars, wind ripples, and desiccation cracks; and 3) an eolian-fluvial interaction plain (Deri and Ciccioli, 2018). In the semi-active to inactive eolian field unit (Fig. 2), small mesoforms develop in the shelter of vegetation, and fossilized dunes (Deri, 2016) where ephemeral fluvial interactions are common.

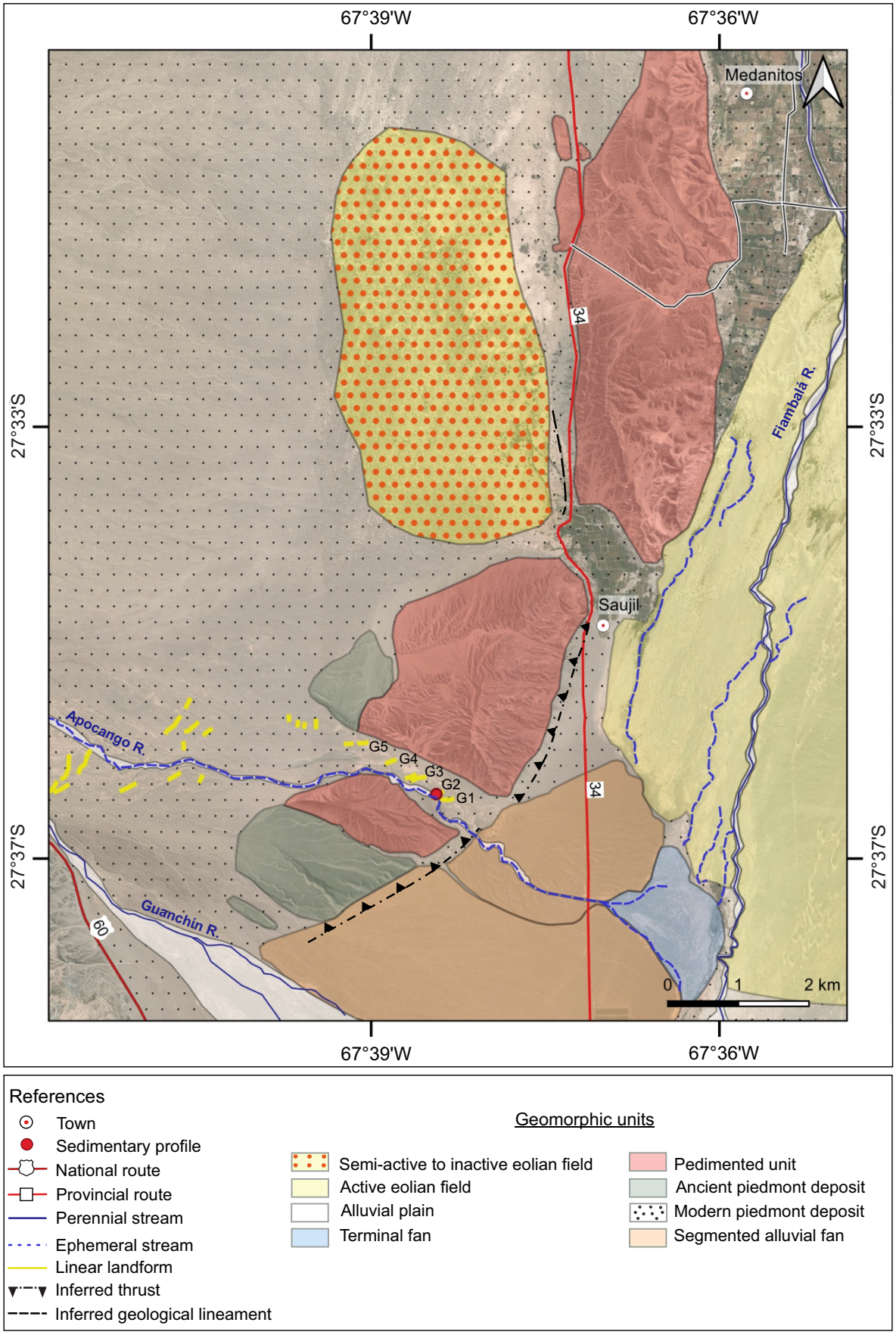

Figure 2. Geomorphological map of the studied area. G1 to G5 indicate sampled landforms.

METHODOLOGY

A general geomorphological and geological mapping of the area was conducted through the visualization and interpretation of satellite images (SENTINEL 2A) and field observations of the geological formations, geomorphic units, and structures. Fieldwork tasks included the description and sampling of the superficial cover of the linear landforms (up to 1 cm depth), general and detailed photographic surveys using a drone (Mavic 2 Pro), and the excavation of three artificial sections. Three samples were taken from the outer superficial cover to a depth of 50 cm from one of the test pits constructed in one of the landforms, where the dry color was determined using the 2009 edition of the Munsell Soil Color Chart.

The climatic conditions of the study area were characterized by analyzing meteorological data from 2019 to 2022, which were obtained from the Pegasus Plus Meteorological Station installed in Medanitos (Fig. 1) by the research team. The wireless meteorological station has sensors for internal and external air temperature, internal and external air humidity, precipitation, wind velocity and direction, gusts, and atmospheric pressure. Data are automatically recorded every 15 minutes and transmitted online for real-time access. Complementary data recorded from 1985-2015 at the Tinogasta station of the National Meteorological Service (Servicio Meteorológico Nacional, 2015), located 50 km south of the study area, were consulted. The mean, minimum, and maximum values of precipitation (mm), temperature (°C), wind velocity (km/h), and gust velocity (km/h) were calculated, from which a series of graphs were made to visualize the data. To assess the wind sand-transport capacity, the method proposed by Fryberger (1979) was applied, which involves calculating the resultant drift direction (RDD) in degrees (°), the drift potential (DP) and the resultant drift potential (RDP) in vector units (VU), and the directional variability of the wind (RDP/DP). In applying Fryberger's (1979) equation, a threshold wind velocity of 6 m/s was used, with measurements expressed in metric units rather than knots (Bullard, 1997). Additionally, wind velocity data were standardized to a height of 10 m above ground level, adjusted from the initial sensor height of 2.5 m, and wind directions were grouped into 16 compass directions.

Two drone flights were conducted using programmed grids created with Pix4Dcapture software for a more detailed morphological analysis. Orthomosaics and digital elevation models (DEMs) were generated from the acquired images using Agisoft Metashape Professional v1.5.0.7011 from which a topographic profile of one of the linear landforms was created.

For textural characterization of the landforms, mechanical analysis of dry sediments (approximately 500 g) of the population of clasts comprised between 32 mm (-5 φ) and 62 μm (4 φ) was conducted, using Tyler-type sieves arranged with a spacing of a whole number of phi of the Udden-Wenthworth grain size scale. The nomenclature proposed by Blair and McPherson (1999) was used for the gravelly fraction, extending the Udden-Wenthworth proposal for this grain size fraction. The units of the artificial section (test pit) were analyzed in detail by sieving 100 to 200 g of sample with a spacing of the fourth root of two of the named granulometric scale. The main statistical parameters were calculated using the moment method: mean (x) and sorting (σ), and graphical measures (Folk and Ward, 1957): mode, median (Md), skewness (SK_1), kurtosis (K_G), and percentile 1% (φ 1%). Dimensions of the major (L), intermediate (I), and minor (S) axes of gravel fraction (of at least 100 clasts per sample) were determined using a vernier caliper. Ternary diagrams (Sneed and Folk, 1958) and visual comparison charts (Pettijhon *et al.*, 1987) were used to obtain shape, sphericity, and roundness.

For a better definition of the surface cover of the linear landforms, morphometric analysis was carried out using high-resolution photographs with an average size of 25 cm x 25 cm of the ridges of the landforms. From the identification and graphical representation of the coarsest granulometric fraction, using the 2Dmeasurement tool of JMicrovision v1.3.4, average values of area (Ac), perimeter (P), length (L), width (W), circularity (C), and roundness (R) were obtained for each clast. In the case of circularity, the relationship between the area and perimeter (Ac/P) of each clast was considered using Cox's equation (1927):

$$C = 4\pi \times \frac{Ac}{P^2}$$

which is a measure of the degree of similarity to a circle. Circularity values fluctuate between 0 (elongated shape, i.e., very low circularity) and 1

(very high circularity). On the other hand, roundness was obtained based on the relationship between the area and the major axis of the clast:

$$R = \frac{4 \times Ac}{\pi \times L^2}$$

(Medina, 2015), the value 0 corresponds to a very angular clast and 1 to a well-rounded one. The obtained values were classified according to Power's proposal (1953). From the ratio of the total area (ATc) of the gravel clasts and the total area of the analyzed photograph (ATf), the percentage of the gravelly fraction vs. intergranular space, which includes the fraction <2 mm, was calculated to characterize the type of packing.

Gravel composition was determined by observing, under a binocular magnifying glass, the previously measured clasts and were classified based on the modified diagram of Limarino *et al.* (1996 in Scasso and Limarino, 1997). For the sand fraction, eight petrographic slides of artificially consolidated samples were observed under a Leica DM750P petrographic microscope, with approximately 300 grains counted per sample. Sands were classified according to Folk *et al.* (1970) proposal, and additional ternary diagrams were generated.

ANALYSIS OF CLIMATIC PARAMETERS

The Fiambalá Valley is located within the climatically dry strip known as the Arid Diagonal (Bruniard, 1982), which extends along the Andes from Ecuador to Patagonia. In the study area, the Andes Mountain range acts as a barrier to the moist westerly winds coming from the Pacific Ocean. Additionally, the area is in a transition zone between these moist westerly winds and the Tropical Monsoonal System (Garleff *et al.*, 1994; Garreaud *et al.*, 2009). Therefore, the region experiences average annual precipitation of less than 100 mm, according to data recorded from 1985-2015 at the Tinogasta meteorological station (28°04'S - 67°34'W; 1201 m.a.s.l), the capital of the department that contains the study area (Servicio Meteorológico Nacional, 2015). These precipitations are concentrated in the summer and are characterized by their torrential nature. The winds have a preferential direction from the SSW, reaching their maximum average velocity of 13.7 km/h in September and October, although gusts between 40 and 100 km/h are frequent (Viera, 1982; Servicio Meteorológico Nacional, 2015; Deri and Ciccioli, 2018).

To better assess the climatic conditions in regions with complex topography like the study area, the current spatial resolution of general circulation models is poor, and therefore, temperature, precipitations, and wind observations recorded by *in situ* meteorological stations are indispensable. The data series from March 2019 to December 2022, obtained from the Pegasus Plus meteorological station in Medanitos (Fig. 1), indicates, there is a dry season from May to August (with up to 1.25 mm of accumulated precipitation, recorded in July 2021) and a wet season from September to April, during which the maximum monthly accumulated precipitation ranges between 13 and 31 mm (Fig. 3a).

The maximum temperatures range around 40.6°C in January, and the minimums reach -8.35°C in July; however, the average temperatures for these months are 25.73°C and 9.94°C, respectively (Fig. 3b). The separation of the maximum and minimum curves in the graph of figure 3b denotes the significant thermal amplitude prevailing throughout the valley.

Regarding the maximum wind velocities and gusts, it was noted that, on average, the months with the highest values are July, June, September, and December, with April and May being the least windy (Fig. 3c). When comparing the curves of maximum wind velocities and gusts, it is observed that they follow a similar pattern, differing in that gusts are almost twice as fast. The average maximum values of wind velocities and gusts recorded in the four years analyzed belong to July and are 44.60 km/h and 65.10 km/h, respectively.

The determination of the average wind directions revealed that, although each year studied has its particularities, the prevailing winds are from the SW, followed by those from the W and NE (Fig. 3d).

The vectorial analysis of wind directions and velocities collected in the Fiambalá Valley (2019 - 2022) indicates a complex to acute bimodal distribution, with a prevailing component from the southwest (SW-WSW) (Fig. 4a), consistent with the observations from the annual seasonal analysis (Fig 3d). The calculation of the resultant drift direction (RDD) is 204.99° suggesting sand transport from the southwest (SW-WSW) towards the northeast (NNE-NE). The drift potential (DP) is estimated at 29.21 VU indicating an intermediate-energy wind environment (Fryberger,1979; Bullard,1997), and the resultant drift potential (RDP) yields 12.33 VU. The directional variability of the wind (RDP/DP) is 0.42 (Fig. 4b), which implies an intermediate variability in wind directions and coincides with the distribution of wind directions shown in figure 4a.

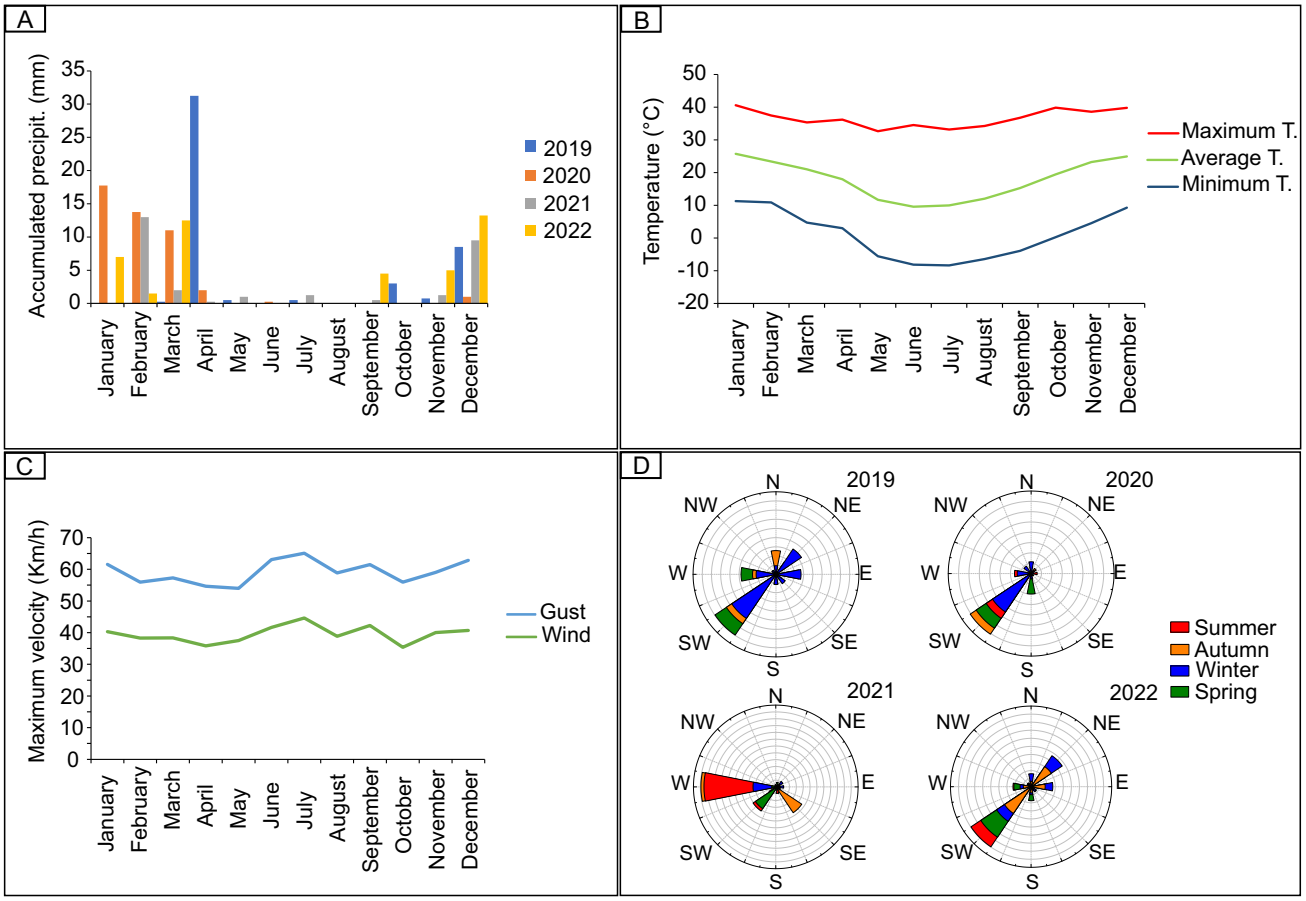

Figure 3. Graphical representations of the results obtained for accumulated precipitation (precipit.), temperature (T), maximum wind velocity, gusts, and wind direction for 2019-2022. **a)** Monthly accumulated precipitation values (mm). **b)** Average temperature values (°C) for each month of the year accompanied by the curves of maximum and minimum values. **c)** Curves of maximum monthly average wind velocity values (Km/h) and gusts. **d)** Wind roses representing the wind directions (°) according to the annual seasons.

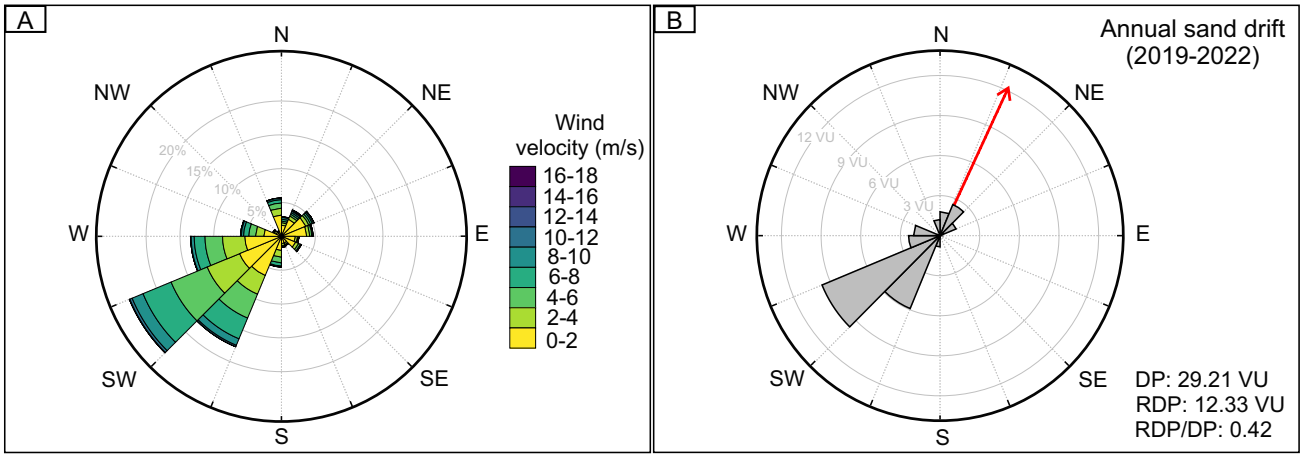

Figure 4. a) Wind rose resulted from analyzing wind directions and velocities (m/s) of the four years studied (2019-2022). **b)** Annual sand drift potential from the vectorial analysis of wind directions and velocities (m/s) using Fryberger's (1979) equation. DP: drift potential (VU), RDP: resultant drift potential (VU), and RDP/DP: directional variability of the wind. The red arrow indicates the resultant drift potential and the direction of sand transport.

Summarizing, the Fiambalá Valley exhibits arid environmental conditions (Meigs, 1953; Grove,1977; MAP: 25 - 200 mm) characterized by significant thermal amplitude, high annual average temperature, scarce and torrential rainfall with a regular seasonal rhythm (Goudie, 2013), and prevailing wind directions from the southwest (SW-WSW), which promotes sand transport toward the northeast (NNE-NE).

IDENTIFICATION OF LINEAR LANDFORMS

Linear landforms were recognized in the narrow gorge delimited by Pliocene-Pleistocene pedimented unit (Rodados de la Puna Formation) and ancient piedmont deposit levels (Table 1, Fig. 2) on the Apocango River terraces; numerous similar morphologies were also identified to the west of that area (Fig. 2). These landforms are characterized by being slightly asymmetric to symmetric in transverse section, with rounded crests (Fig. 5), an average height between 0.3 and 3.5 m, a width from 8 to 14.5 m, and a length between 34 and 118 m. They are arranged as isolated bodies with an average spacing of 81.05 ± 21.73 m and straight to slightly sinuous ridges of approximately NE-E to SW-W direction (~ 67°- 108°) (Fig. 2 and 5c).

These landforms are partially degraded by human activity, due to vehicle use, and by deflation processes (Fig. 5a and b). They have a superficial covering that is, on average, 3 cm thick.

Sample	Localization	Height (m)	Width (m)	Length (m)	Azimuth (°)
G1	27°36'8.8"S 67°38'23.4"W	3.50	14.50	95.00	108
G2	27°36'6.3"S 67°38'25.1"W	2.10	9.80	34.01	82
G3	27°35'58.6"S 67°38'39"W	0.30	8.83	112.69	70
G4	27°35'51.4"S 67°38'49.4"W	1.00	7.72	118.00	67
G5	27°35'43.1"S 67°39'5.2"W	0.60	8.18	82.00	96

Table 1. Principal morphological characteristics of the linear landforms analyzed.

Textural analysis of the superficial cover

From the granulometric analysis of the sample superficial cover of the landforms (G1, G2, G3, G4, and G5 from Fig. 2), it was obtained that the sediments present an average grain size of medium pebble to very coarse sand (x: -3.6 to -0.85 φ; Table 2). The grain size frequency distribution is bimodal with a primary mode in the medium to coarse pebble fraction (-4.5 to -3.5 φ) and a secondary one in fine sand (2.5 φ); it is very platykurtic to platykurtic (K_g: 0.6 - 0.88), except for G3 that shows an extremely leptokurtic frequency curve (K_g: 8.16). The sediments are very poorly sorted (σ: 2 - 3.03) with very fine skewness (SK_1: 0.32 - 1) (Fig. 6). Median range from medium-coarse pebble to granule (-4 to -1.45 φ) and percentile 1% is coarse pebble (φ 1%: -4.91 to -4.98 φ).

Although the pebble fraction is predominant (P: 47.19 - 89.88%), it was observed that fine sand follows in abundancy (Sf: 1.96 - 14.68 %), then medium sand (Sm: 1.40 - 8.93%) and mud (Z-C: 2.34 - 6.64%); being minority the fraction of granule (G: 1.56 - 7.87%), coarse sand (Sc: 1.17 - 6.71%), very coarse sand (Svc: 1.25% - 5.35%) and very fine sand (Svf: 0.44% - 5.65%) (Table 3).

The study of the gravelly fraction of the superficial cover of the landforms was approached using the vernier caliper to analyze them texturally and morphologically (Table 4). According to the categories of Pettijhon *et al.* (1987), the clasts are on average sub-rounded (ρ: 3.40), with moderate sphericity since they present average sphericity values between 0.72 and 0.77 (Table 4, Fig. 7). The predominant shapes are compact-elongate (20.4%), compact-bladed (20.2%), compact (15.4%), bladed (13.2%), compact-platy (11.8%) and elongate (11.2%), and, to a lesser extent, platy (5.2%), very bladed (1.8%) and very elongate together with very platy (0.8%) (Table 4, Fig. 7).

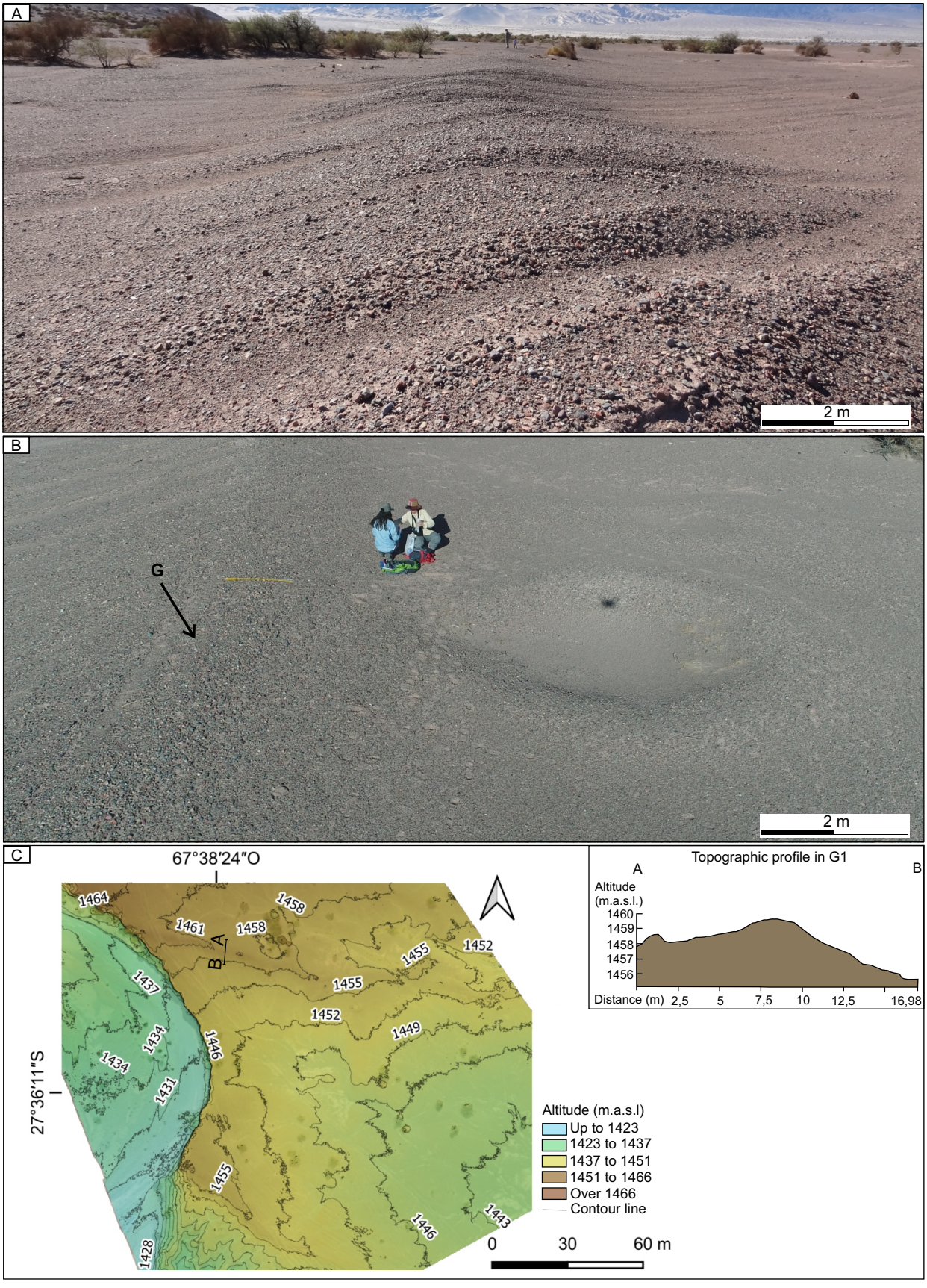

Figure 5. a) Image of one of the landforms studied with anthropic degradation. **b)** Image showing a deflation hole and a linear landform (G) **c)** DEM superimposed on orthomosaic and topographic profile in linear landform G1 taken from the DEM (A-B).

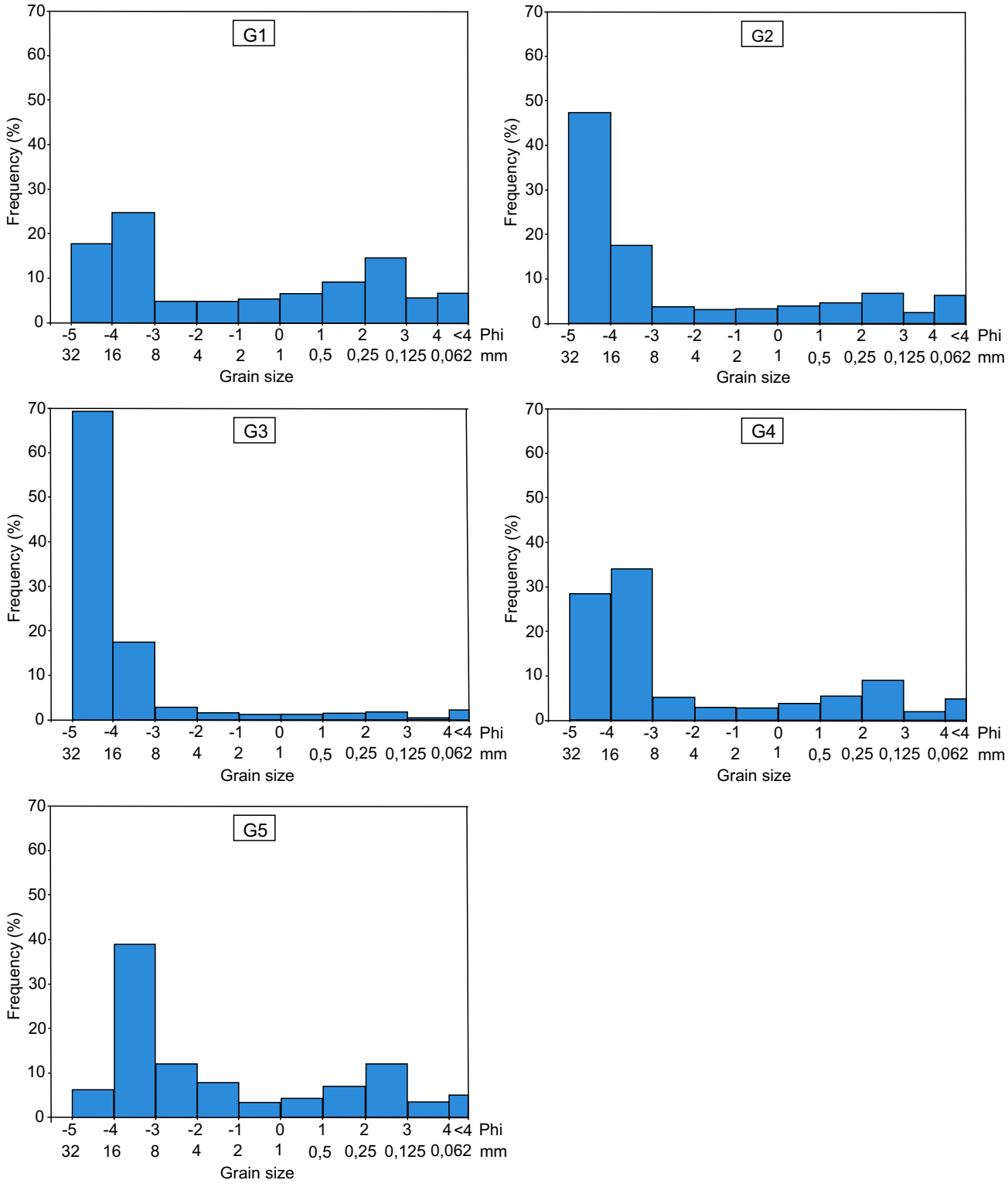

Figure 6. Frequency histograms of the respective sample cover of the analyzed landforms: G1, G2, G3, G4, and G5.

Sample	Mean	Sorting	Mode		Skewness	Kurtosis	Median	1% percentil
	X (Phi)	σ	Primary (Phi)	Secondary (Phi)	Sk_1	K_g	Md (Phi)	φ 1% (Phi)
G1	-0.85	3.03	-3.50	2.50	0.32	0.6	-1.45	-4.95
G2	-2.29	3.00	-4.50	2.50	0.99	0.88	-3.98	-4.96
G3	-3.60	2.00	-4.50	-----	1.00	8.16	-4.00	-4.97
G4	-2.10	2.80	-3.50	2.50	0.81	0.81	-3.36	-4.98
G5	-1.30	2.80	-3.50	2.50	0.64	0.70	-2.57	-4.91

Table 2. Statistical granulometric parameters of each analyzed landform.

Sample	Gravel		Sand					Mud
	P (%)	G (%)	Svc (%)	Sc (%)	Sm (%)	Sf (%)	Svf (%)	Z-C (%)
G1	47.19	4.85	5.35	6.71	8.93	14.68	5.65	6.64
G2	69.11	3.28	3.32	3.97	4.68	6.84	2.50	6.30
G3	89.88	1.56	1.25	1.17	1.40	1.96	0.44	2.34
G4	68.53	3.04	2.92	3.88	5.54	9.13	2.01	4.95
G5	56.77	7.87	3.39	4.38	7.09	11.88	3.55	5.07

Table 3. Relative frequencies by granulometric fraction. References: P: pebble, G: granule, Svc: very coarse sand, Sc: coarse sand, Sm: medium sand, Sf: fine sand, Svf: very fine sand, and Z-C: silt-clay.

Analysis of images of the sandy gravel superficial cover

The superficial cover of the linear landforms (samples G1, G2, G3, G4, G5) was also studied through image analysis based on high-resolution photographs taken in the field. Average values of area (Ac), perimeter (P), length (L), width (W), circularity (C), and roundness (R) were obtained for each clast. Also, the percentage of the gravelly fraction vs. intergranular space was calculated (Table 5, Fig. 8).

In sample G1 taken from landform one, 965 clasts were recognized (Fig. 8), with an average clasts area (Ac) of 0.35 cm^2, representing a total area (ATc) of 335.10 cm^2. It was found that the clasts, on average, exhibit high circularity (0.82). They are well-rounded to sub-rounded, with an average roundness of 0.60. The gravelly fraction represents 44.49% of the analyzed photograph, and the remaining 55.51% corresponds to intergranular space.

In sample G2 taken from landform two, 1020 clasts were identified (Fig. 8), with an average clasts area (Ac) of 0.35 cm^2 and a total area (ATc) of 358.86 cm^2. It was determined that 46.59% are gravel-sized clastic components, and 53.41% corresponds to intergranular space. The clasts exhibit an average circularity of 0.80 and are sub-rounded to well-rounded, with an average roundness of 0.58.

For linear landform three (sample G3), 540 clasts were recognized with an average area (Ac) of 0.74 cm^2 and a total area (ATc) of 399.15 cm^2, implying that 58.60% corresponds to the gravelly fraction and 41.40% to intergranular space. The clasts exhibit an average circularity of 0.84 and are well-rounded to sub-rounded, with an average roundness of 0.62 (Fig. 8).

In the case of landform four (sample G4), 821 clasts could be delimited with an average area (Ac) and total area (ATc) of 0.42 cm^2 and 341.14 cm^2, respectively. They exhibit high circularity on average (0.84) and are well-rounded to sub-rounded, with an average roundness of 0.64. The gravel-sized clastic components comprise 49.39%, and the remaining 50.61% corresponds to intergranular space (Fig. 8).

Finally, the analysis of landform five (sample G5) resulted in the identification of 1376 clasts with an average area (Ac) and total area (ATc) of 0.24 cm^2 and 326.67 cm^2, respectively. They have high circularity on average (0.84) and are well-rounded

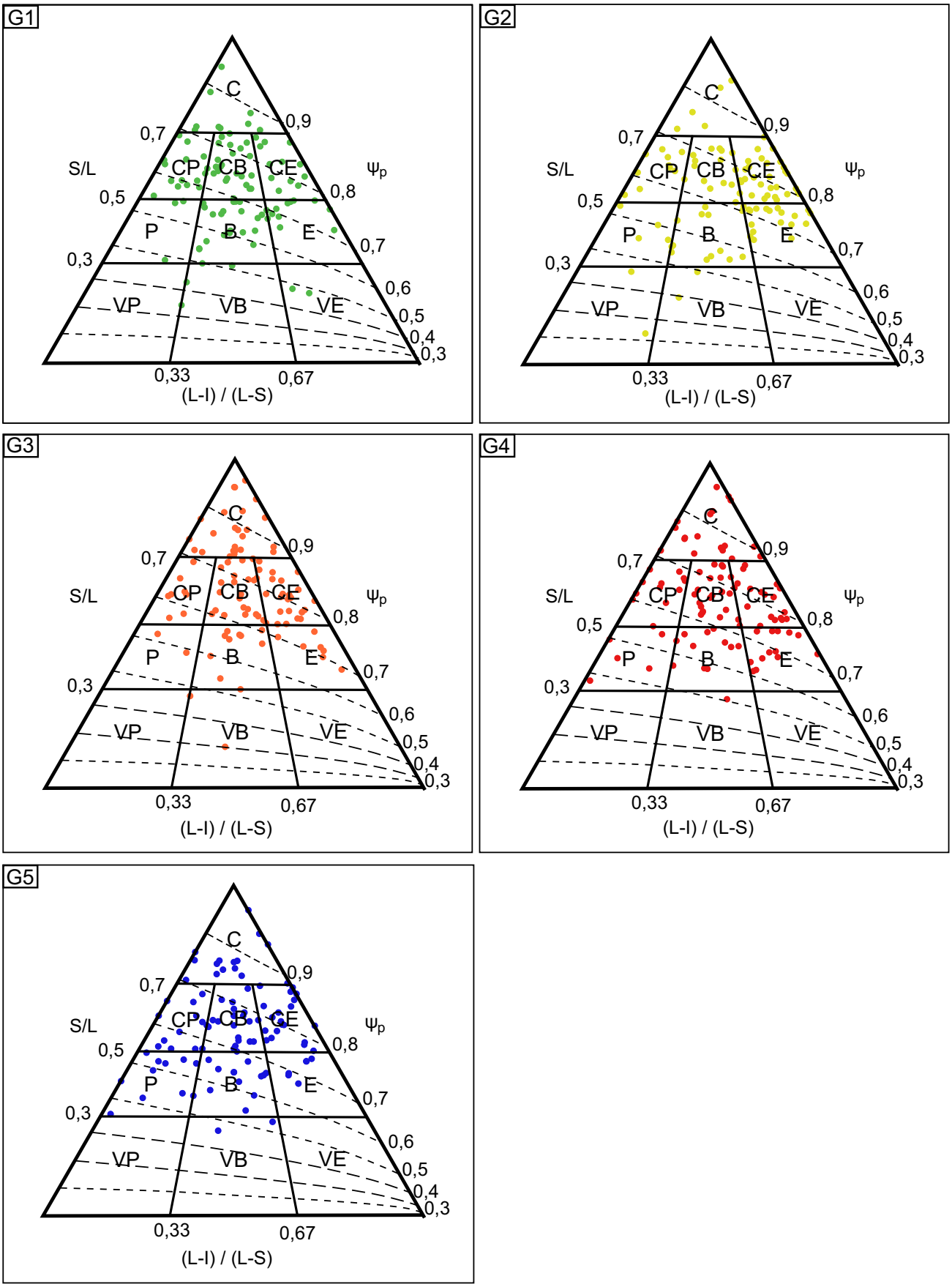

Figure 7. Ternary diagrams of Sneed and Folk (1958) for shape classes and isosphericity curves (ψp). C: compact, CP: compact-platy, CB: compact-bladed, CE: compact-elongate, P: platy, B: bladed, E: elongate, VP: very platy, VB: very bladed, and VE: very elongate.

to sub-rounded, resulting in an average roundness of 0.63. 48.28% corresponds to the gravelly fraction, and 51.72% to intergranular space (Fig. 8).

In summary, the studied landforms consist of 44.49 to 58.60% gravel-sized clasts and 41.40 to 55.51% of intergranular space, suggesting an open to moderate packing (Fig. 8). The clasts present on average an area with values between 0.24 and 0.74 cm^2, a perimeter of 1.71 to 2.83 cm and a length and width of 0.64 to 1.06 cm and 0.41 to 0.71 cm, respectively. As for circularity, this yielded average values of 0.80 to 0.84, while the average roundness is 0.58 to 0.64. This implies that the clasts have a high circularity and are rounded.

Sample	Shape (%)										Sphericity	Roundness
	C	CP	CB	CE	P	B	E	VP	VB		ψ	ρ
G1	11	15	23	14	2	21	10	0	2	2	0.72	3.33
G2	6	11	15	28	5	12	19	2	2	0	0.73	3.42
G3	27	8	21	23	2	10	7	0	2	0	0.77	3.49
G4	18	12	22	18	6	10	13	0	1	0	0.75	3.37
G5	15	13	20	19	11	13	7	0	2	0	0.73	3.39
Average	15.4	11.8	20.2	20.4	5.2	13.2	11.2	0.4	1.8	0.4	0.74	3.40

Table 4. Morphological parameters of the different populations of clasts. C: compact, CP: compact-platy, CB: compact-bladed, CE: compact-elongate, P: platy, B: bladed, E: elongate, VP: very platy, VB: very bladed, and VE: very elongate.

Sample	Ac (cm^2)	ATc (cm^2)	ATf (cm^2)	P (cm)	L (cm)	W (cm)	C	R	Gravelly fraction (%)
G1	0.35	335.10	753.12	1.78	0.67	0.43	0.82	0.60	44.49
G2	0.35	358.86	770.19	1.72	0.64	0.41	0.80	0.58	46.59
G3	0.74	399.15	681.13	2.83	1.06	0.71	0.84	0.62	58.60
G4	0.42	341.14	690.69	2.16	0.80	0.54	0.84	0.64	49.39
G5	0.24	326.67	676.65	1.71	0.64	0.42	0.84	0.63	48.28

Table 5. Results of the values obtained from the graphical representation of the coarsest granulometric fraction with JMicrovision software: Ac: average area of clasts, ATc: total area of gravel clasts, ATf: total area of the analyzed photograph, P: perimeter, L: length, W: width, C: circularity, R: average roundness of clasts and percentage of gravelly fraction.

Textural analysis of the internal part

For a better textural characterization of the linear landforms, a transverse profile was made in landform two (Fig. 2) based on one of the excavations done. It extends from the superficial cover to a depth of 50 cm (units 1 to 4 where U4 is equivalent to G2, Fig. 9). The profile's base is covered, and four units were identified from base to top (Fig. 9a and b). Unit 1 (U1), 15 cm thick, has tabular geometry, massive structure, probably due to pedogenic processes, and brownish color (7.5YR 5/2); it consists of slightly gravelly muddy fine sand (SFm, x: 2.41 φ, Fig. 9c). It is composed of 73.95% sand, 16.57% mud, and 9.48% gravel with a bimodal distribution with a primary mode in fine sand (2.88 φ) and secondary in fine pebble (-2.5 φ), poorly sorted (σ: 1.93; Table 6).

Unit 2 (U2), 15 cm thick, presents tabular geometry, brownish color (7.5YR 5/2), and a slightly horizontal to low-angle lamination, or a massive structure; it is composed of gravelly sand (SGm/SGh), where 64.28% of the sample corresponds to sand size, 28.01% to gravel and 7.71% to mud (Fig. 9c). The statistical parameters indicate that it presents a mean in medium sand (x: 1.31 φ) and a bimodal grain size distribution with a primary mode in granule (-1.13 φ) and two secondaries: one in fine pebble (-2.5 φ) and another in fine sand (2.88 φ). In addition, it presents a very poor selection (σ: 2.18; Table 6).

Finally, overlying U2 and beneath the sandy gravel superficial cover (U4), there is Unit 3 (U3), consisting of 15 cm of muddy fine sand (x: 2.66 φ and mode: 2.88 φ) with scattered fine pebble-sized particles, a light brownish gray color (10YR 6/2), and a massive structure (SFm). It comprises 79.05% sand, 16.19% mud, and 4.76% gravel, exhibiting a unimodal grain size distribution and poor sorting (σ: 1.58; Table 6, Fig. 9c).

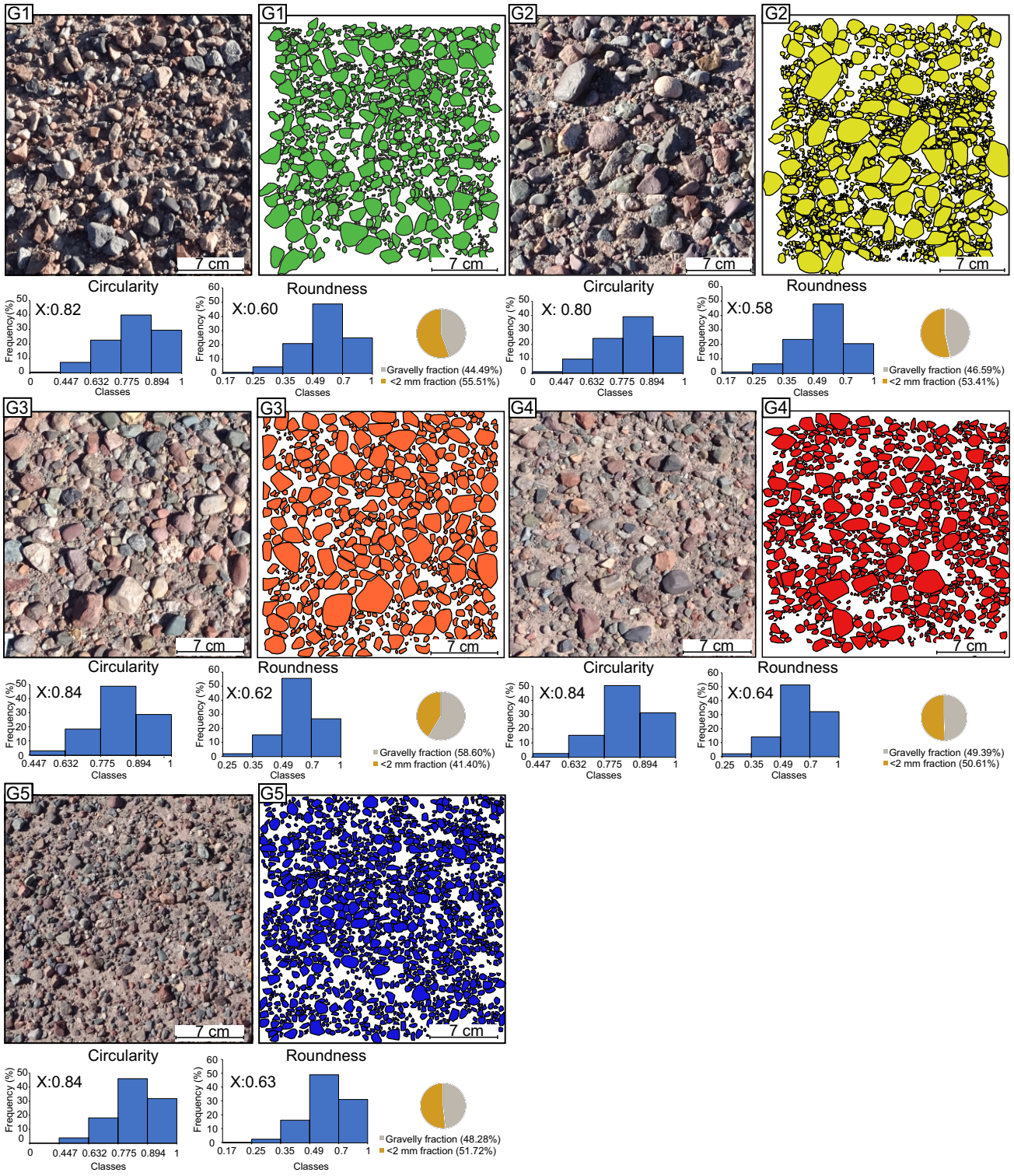

Figure 8. Photographs of the sandy gravel superficial cover of the linear landforms (G1 to G5) and their respective images analyzed with JMicrovision software, where the gravelly fraction is represented.

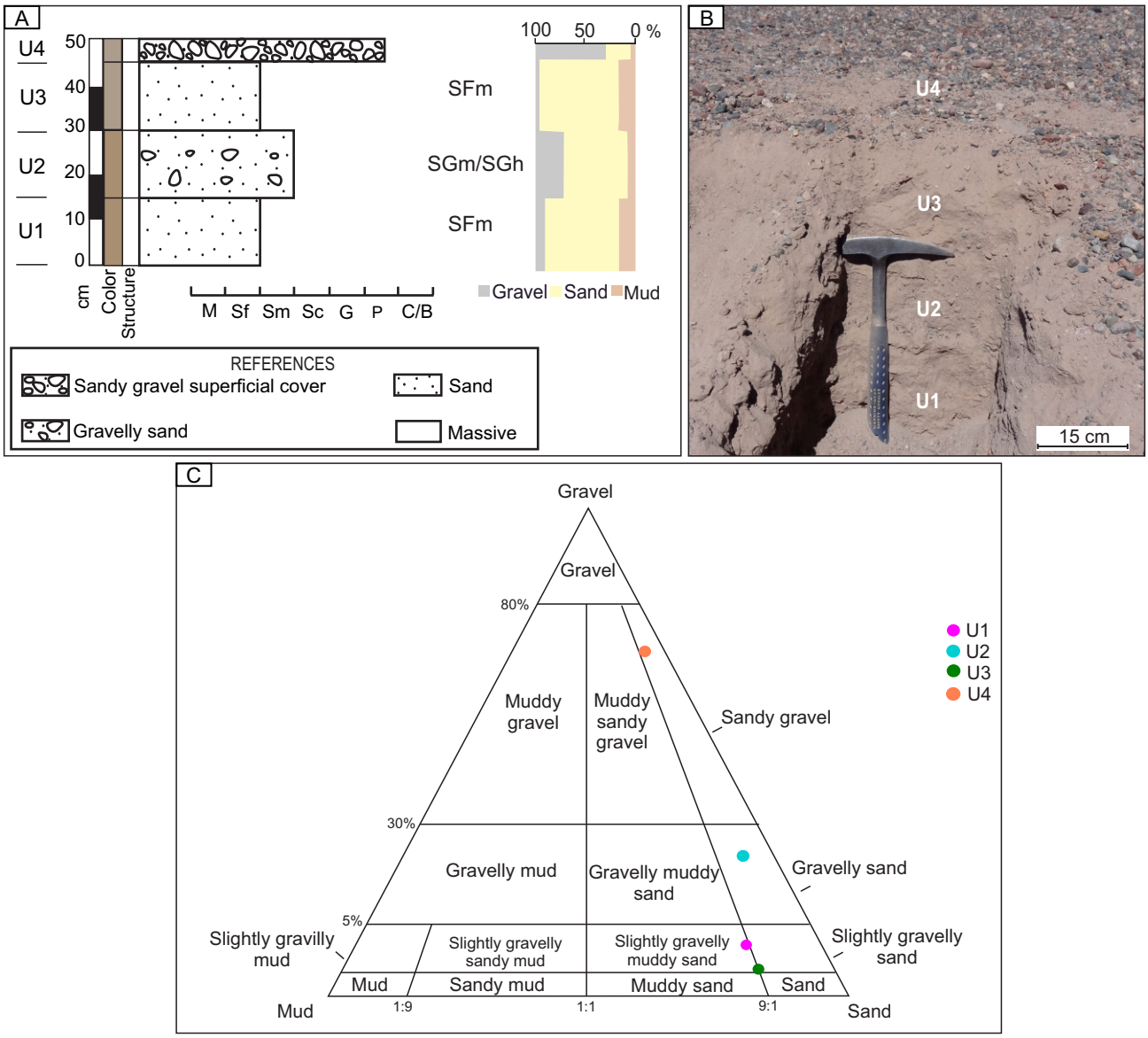

Figure 9. a) Sedimentological profile of linear landform two (U: unit). **b)** Units recognized in the artificial section (U: unit). **c)** Ternary diagram of textural classification of the units of the profile analyzed according to Folk (1954).

Sample	Mean	Sorting	Mode		Skewness	Kurtosis	Median	1% percentil
	X (Phi)	σ	Primary (Phi)	Secondary (Phi)	Sk_1	K_g	Md (Phi)	φ 1% (Phi)
U3	2.66	1.58	2.88	-----	-0.26	1.37	2.89	-2.27
U2	1.31	2.18	-1.13	-2.50 y 2.88	-0.28	0.63	1.90	-2.99
U1	2.41	1.93	2.88	-2.50	-0.38	1.36	2.87	-2.98

Table 6. Statistical granulometric parameters of the units recognized in the profile carried out in landform two.

Compositional analysis

For the compositional analysis of the linear landforms (samples G1 to G5), the gravelly fraction was characterized using a binocular magnifying glass, along with a study of detrital modes of the sandy fraction of both the superficial cover and the internal part of the landforms.

Regarding the gravelly fraction, it was recognized that compositionally the clasts of green sedimentary lithics (22.92 - 32.72%) dominate, followed by acid volcanic lithics (15 - 21.49%), purple sedimentary lithics (13.72 - 17.04%), basic (10.60 - 17.78%) and intermediate volcanic lithics (9.74% - 12.93%), and subordinately granites (2.57 - 8.61%), quartzites (2.61 - 6.07%), quartz (0 - 5.86%), orange sedimentary lithics (0 - 6.59%) and metamorphic lithics (0 - 2.01%). According to their composition, they are classified as lithic gravels as proposed by Limarino *et al.* (1996 in Scasso and Limarino, 1997) (Fig. 10).

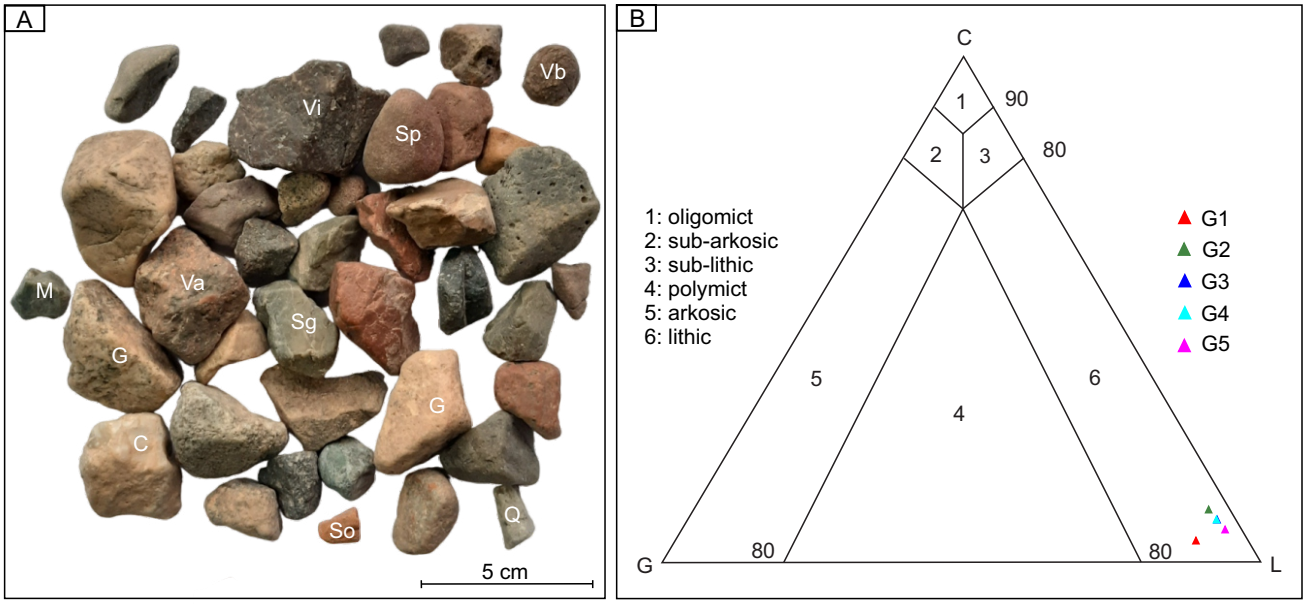

Figure 10. a) Photograph of the main lithological components of the gravel fraction. Sg: green sedimentary lithic, So: orange sedimentary lithic, Sp: purple sedimentary lithic, Va: acid volcanic lithic, Vi: intermediate volcanic lithic, Vb: basic volcanic lithic, M: metamorphic lithic, Q: quartz, C: quartzite, G: granite. **b)** Classification diagram modified from Limarino *et al.* (1996 in Scasso and Limarino,1997).

Petrographic analysis of the eight sand samples, both from the surface of the landforms and the internal part (profile units, Table 7), revealed that lithic fragments are the dominant component (L: 35.71 - 47.51%), followed by quartz (Q: 23.59 - 37.92%), and finally feldspars (F: 19.80 - 32.76%) (Fig. 11). The lithic fragments were classified as volcanic lithics (Lv: 27.41 - 37.70%), metamorphic-plutonic lithics (Lm+Lp: 2.62 - 7.01%), and sedimentary lithics (Ls: 2.61 - 5.92%). Within the volcanic lithics, three types were recognized: 1. those of acidic composition, which are the majority component (Lvf/m: 20.06 - 31.15%) and are characterized by volcanic pastes with microgranular or felsitic textures; 2. the glassy ones, consisting of blocky, non-blocky, and fibrovesicular pumices (Lvv: 1.64 - 10.63%); and 3. the basic ones (Lvi: 0 - 2.55%), with intersertal or intergranular paste textures. Within the metamorphic and plutonic lithic group, it was observed that acidic plutonics (Lpa) are the majority component representing between 1.56 and 6.37% of the total sample, which have a granular texture generally composed of quartz, feldspars, plagioclase, and phyllosilicates; next are the medium to high-grade metamorphics (Lmm/a: 0.31 - 2.18%) corresponding to amphibolites or schists, and finally, the low-grade ones (phyllite and shales) with values ranging from 0 to 0.65%. Regarding sedimentary lithics, the following types were identified: sandstones (Lss: 1.23 - 2.21%), sandstones with iron oxide coating (Lsso: 0.63 - 1.94%), mudstones (Lsp: 0 - 2.80%), and limestone (Lsc: 0 - 0.62%). On the other

hand, quartz is mainly composed of monocrystalline quartz (Qm: 17.83 - 32.69%), followed by mylonitic (Qpm: 0.31 - 2.55%) and granular (Qpg: 0.31 - 2.28%) polycrystalline quartz. As for feldspars, the potassium (K) content varies between 12.94 and 25%, including orthoclase and microcline types, as well as specimens with perthitic and graphic microtextures. Plagioclase (P), which presents its typical tabular habit and polysynthetic twinning or zoned, constitutes between 5.86 and 8.79%. Accessory minerals were identified in proportions ranging from 3.13% to 5.30%.

Samples were classified according to the proposal of Folk *et al.* (1970) as feldspathic litharenites (Fig. 12a). Given the abundance of lithic fragments, a ternary diagram was proposed, considering the different types of lithics (Lm+Lp, Ls, and Lv, in Fig. 12b). In this diagram, the predominance of volcanic lithics is evident; therefore, the different varieties of these components were graphed according to the composition of the pastes (Lvv, Lvi, and Lvf/m), indicating that those of acidic composition with felsitic and microgranular pastes are dominant (Fig. 12c).

INTERPRETATION AND DISCUSSION

The studied linear landforms are straight to slightly sinuous ridges, oriented NE-E to SW-W, generally following the prevailing SW-WSW winds (Fig. 4 and 5c), with an average spacing of 81.05 ± 21.73 m. They range from 0.3 to 3.5 m in height and from 8 to 14.5 m in width and feature a bimodal grain size distribution: the superficial cover consists of medium to coarse pebble (-4.5 to -3.5 φ) and fine sand (2.5 φ), while the inner part is made up of fine to medium sand (x: 2.66 - 1.31 φ).

The characteristics of the superficial cover of these landforms, where the coarser particles exhibit an open to moderate packing (44.49 to 58.60%), allow the interpretation of these levels as poorly evolved (immature or incipient) desert pavement (Cooke *et al.*, 1993). This surface is composed of sub-rounded gravels with a thickness of one or two clasts over a mantle of finer material (Mabbutt, 1965, 1977; Cooke and Warren, 1973; Dixon, 2009). This gravelly clastic surface acts as a protective layer for the underlying sediments, providing a substrate for capturing wind-blown sands, silt, and clay (Cooke *et al.*, 1993). Dixon (2009) considers that five main mechanisms

Sample	Qm	Qpg	Qpm	K	P	Lvv	Lvf/m	Lvi	Lpa	Lmb	Lmm/a	Lss	Lsso	Lsp	Lsc	Acc	Q	F	L
G1	17.83	2.23	2.55	19.43	8.28	5.10	27.71	2.55	6.37	0.32	0.32	1.27	1.27	0.32	0.32	4.14	23.59	28.90	47.51
G2	20.85	2.28	0.65	22.48	8.79	3.91	27.69	0.98	3.58	0.65	0.98	1.30	0.98	-	0.33	4.56	24.91	32.76	42.32
G3	30.53	0.31	0.31	19.00	7.48	2.80	23.99	0.62	1.56	-	2.18	1.56	1.25	2.80	0.31	5.30	32.89	27.96	39.14
G4	24.69	1.25	0.31	20.00	6.56	4.69	28.75	2.19	3.13	0.63	0.94	1.56	1.25	0.63	0.31	3.13	27.10	27.42	45.48
G5	32.69	1.62	2.27	12.94	6.15	1.94	27.51	1.29	2.91	0.32	1.94	2.91	1.94	-	-	3.56	37.92	19.80	42.28
U3	26.54	1.85	1.85	25.00	5.86	7.41	20.06	-	1.85	-	0.93	1.23	1.54	0.31	0.62	4.94	31.82	32.47	35.71
U2	26.23	1.64	2.30	15.41	7.54	5.90	31.15	0.66	1.97	0.33	0.33	1.31	0.98	-	0.33	3.93	31.40	23.89	44.71
U1	23.13	1.25	1.88	19.06	6.88	10.63	24.69	1.88	2.50	0.31	0.31	1.56	0.63	0.63	0.31	4.38	27.45	27.12	45.42

Table 7. Compositional count results. Qm: monocrystalline quartz, Qpg: granular polycrystalline quartz, Qpm: mylonitic polycrystalline quartz, K: potassium feldspar, P: plagioclase, Lvv: glassy volcanic lithic fragment, Lvf/m: volcanic lithic fragment with felsitic to microgranular paste, Lvi: volcanic lithic fragment with intergranular to intersertal paste, Lpa: acid plutonic lithic fragment, Lmb: low-grade metamorphic lithic fragment, Lmm/a: medium to high-grade metamorphic lithic fragment, Lss: sandstone lithic fragment, Lsso: sandstone lithic fragment with iron oxide coating, Lsp: mudstone lithic fragment, Lsc: limestone lithic fragment and Acc: accessory minerals. Q (quartz), F (feldspar), L (lithic) according to Folk *et al.* (1970).

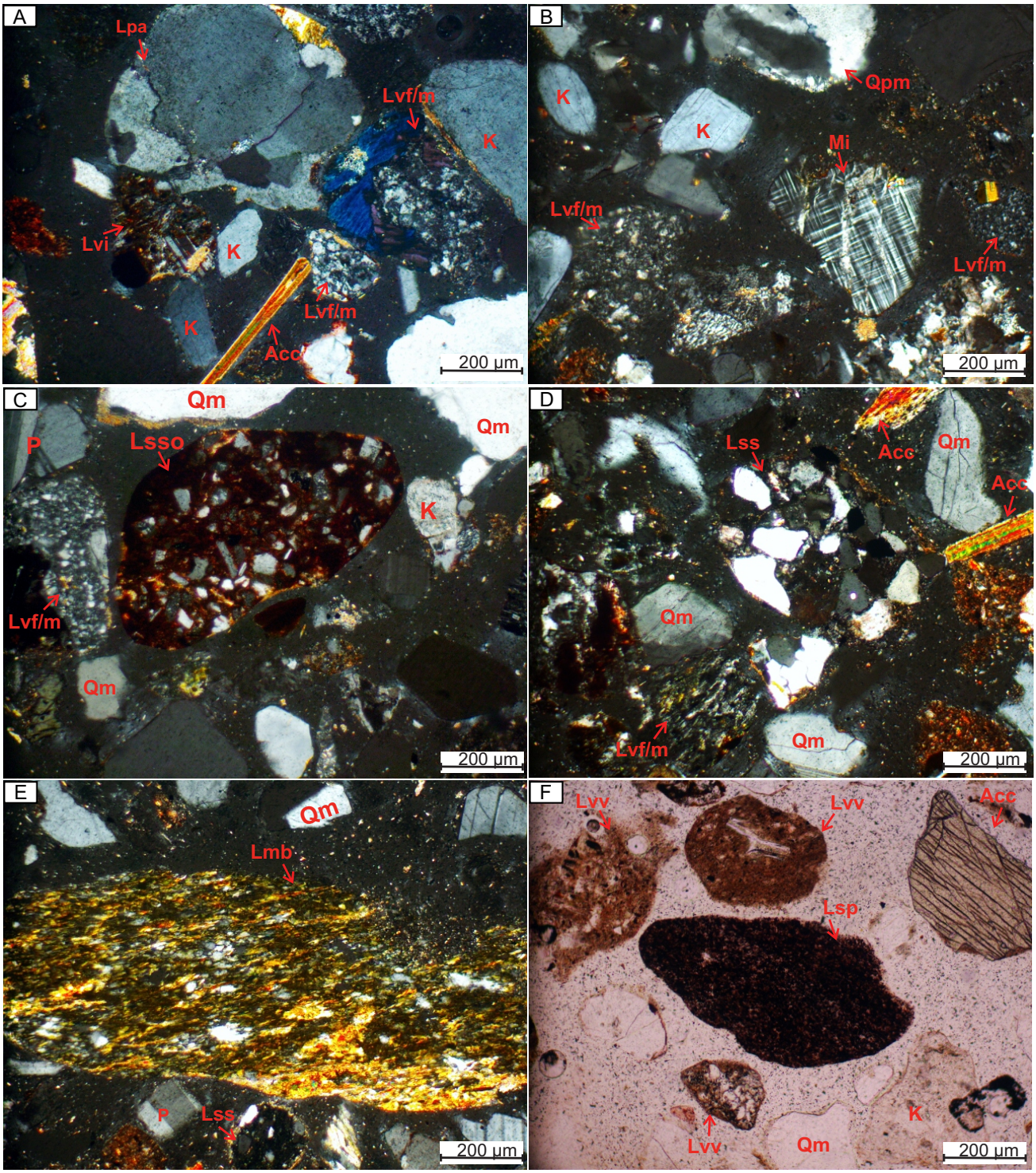

Figure 11. Recognized modal components. **a)** Acid plutonic lithic fragment (Lpa), K-feldspar -orthoclase- (K), and volcanic lithic fragments with felsitic to microgranular (Lvf/m) and integranular to intersertal (Lvi) pastes. **b)** Mylonitic polycrystalline quartz (Qpm) and K-feldspars, both orthoclase (K) and microcline (Mi). **c)** Sandstone lithic fragment with iron oxide coating (Lsso). **d)** Sandstone lithic fragment (Lss) and monocrystalline quartz (Qm). **e)** Low-grade metamorphic lithic fragment (Lmb) and plagioclase. **f)** Glassy volcanic (Lvv) and mudstone (Lsp) lithic fragments, and high-relief accessory minerals (Acc).

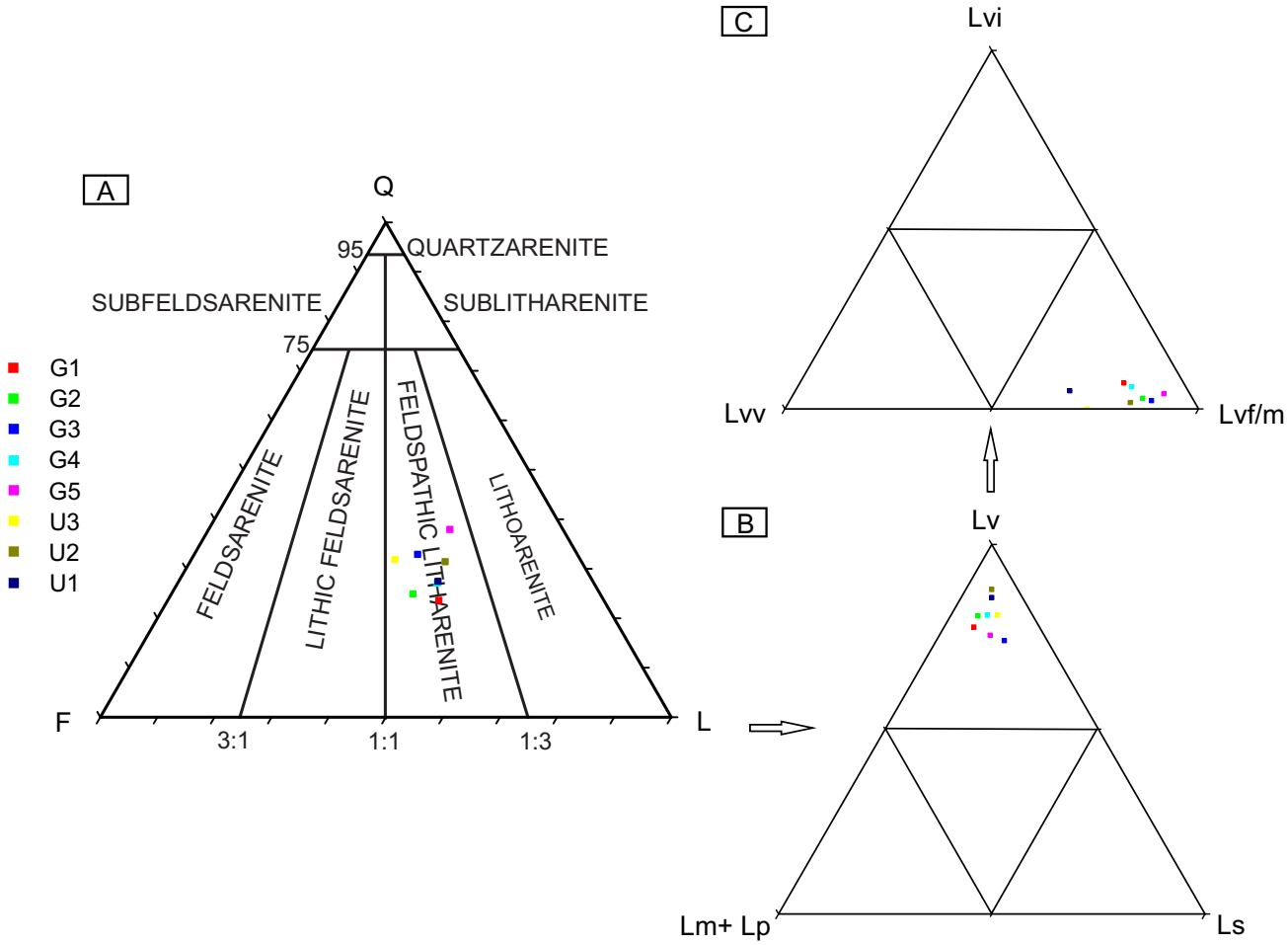

Figure 12. a) Ternary diagram of sand classification according to Folk *et al.* (1970). **b)** Ternary diagram where the types of lithics are discriminated: metamorphic and plutonic (Lm+Lp), sedimentary (Ls) and volcanic (Lv). **c)** Diagram that discriminates the volcanic lithics in glassy (Lvv), with felsitic or microgranular paste (Lvf/m), and those with intergranular to intersertal paste (Lvi).

give rise to desert pavements, with deflation being the most common. In this process the wind removes finer material, leaving gravel clasts that form a lag deposit. Regarding the possible origin of the gravelly material, Dixon (2009) suggests a connection to fluvial sediments from adjacent courses or the physical weathering of nearby rock bodies. In this context, the compositional analysis of the gravels, with a predominance of green sedimentary lithics, acid volcanic lithics, purple sedimentary lithics, and basic and intermediate volcanic lithics, aligns with this hypothesis. This composition indicates that the gravelly material originates from the west (Sistema de Famatina), coinciding with the source area of the Apocango fluvial system, and the physical weathering of the Pliocene-Pleistocene pedimented unit (Rodados de la Puna Formation) surrounding the area.

Based on the analysis of the internal section of the linear landforms, it was recognized that they exhibit a structure ranging from slightly horizontal to low-angle lamination or massive. The horizontal to low-angle lamination is interpreted as a result of wind ripple migration (Hunter, 1977), while the massive structure is associated with pedogenic activity that altered the original characteristics (Retallack, 2001).

The sandy sediment, corresponding to feldspathic litharenites with abundant volcanic lithic fragments, mainly acidic, in addition to feldspars, would also indicate the Sistema de Famatina as the main source, which agrees with the preferential directions of wind that transport the material from the SW-WSW towards the NNE-NE. In this sense, the scarcity of glassy volcanic lithic fragments (pumiceous fragments and shards), abundant components in the Medanitos (Deri and Ciccioli, 2017, 2018) and

Tatón (Isla and Espinoza, 2017; Isla *et al.*, 2021) dune fields, stands out. This could be indicating not only the lower contribution from the Puna but rather the importance of deflation in the study area, since due to the lower density of glassy particles they are quickly and easily deflated and deposited in the sandy eolian accumulations that have developed in the center and east of the valley (Fig. 1 and 13).

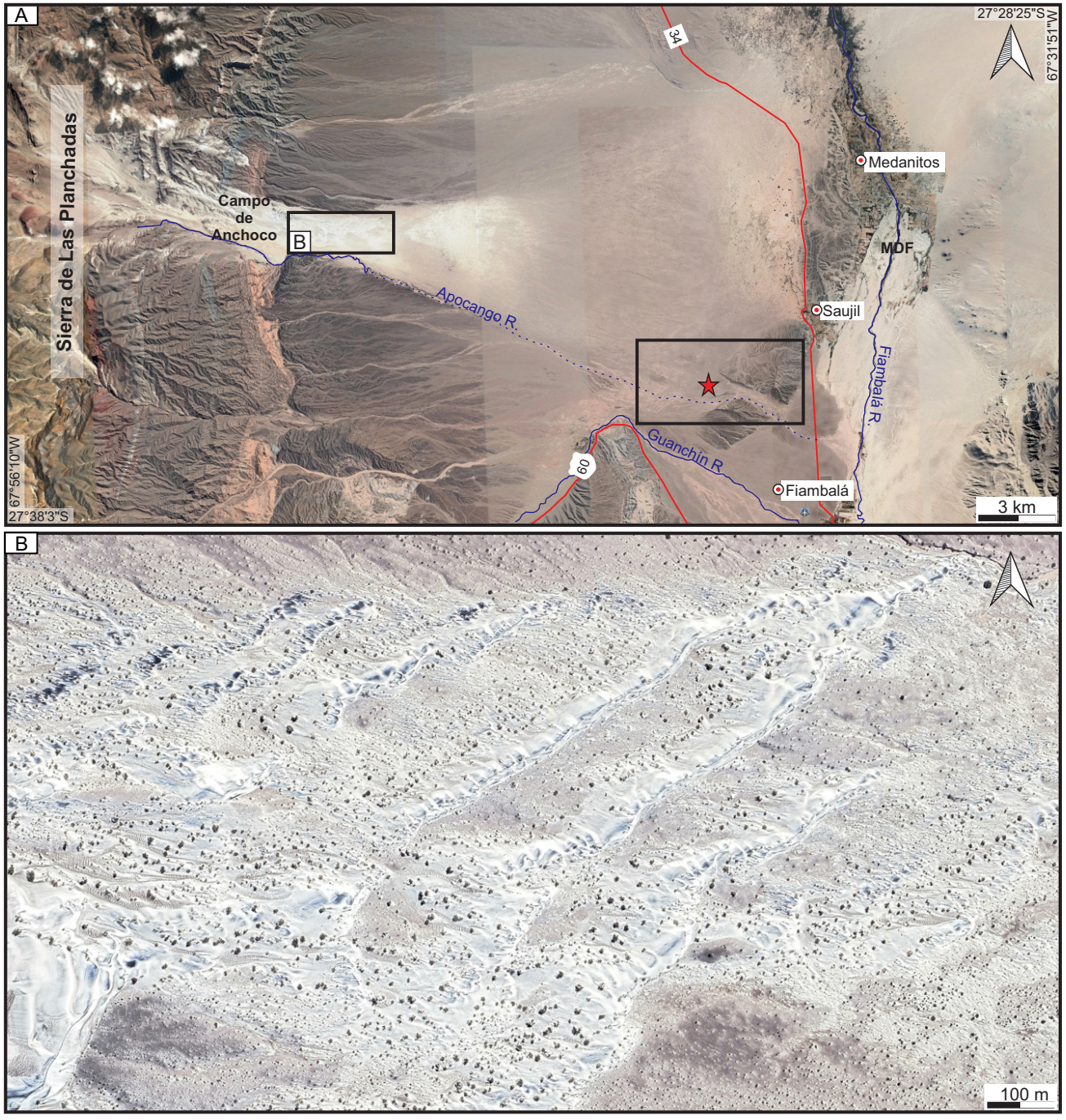

Figure 13. a) General map with the studied area marked with a red star and the Campo de Anchoco dunes. MDF: Medanitos dune field. **b)** Detail of the dunes developed at the Campo de Anchoco site.

Given that the height/width ratio of the linear landforms studied here ranges from 0.04 to 0.24, consistent with those calculated for megaripples and dunes by Zimbelman *et al.* (2012), it could be concluded that these morphologies can be characterized using either term.

Megaripples are characterized primarily by being transverse to the preferential winds, a bimodal granulometric distribution of coarse particles, ranging from very coarse sand to very coarse pebbles and fine particles (fine to medium sand) (Yizhaq *et al.*, 2009; Milana, 2009; De Silva *et al.*, 2013; Lämmel *et al.*, 2018), with a larger scale than sand ripples, and decimeters to decameters spacing (Gough *et al.*, 2020).

On the other hand, linear dunes, are distinguished by their straightness and parallelism (Lancaster, 1995; Pye and Tsoar, 2009). Like other dune types, there are three varieties: simple, complex, and compound. Simple linear dunes consist of a single narrow dune with straight to slightly sinuous, parallel to sub-parallel ridges. These ridges may be rounded in cross-section and with their axes aligned parallel to the resultant drift direction (RDD). They are commonly found in environments with intermediate directional variability, where the RDP/DP ratio ranges from 0.3 to 0.8 (Fryberger, 1979). In nature, we can recognize two main types: vegetated dunes with more rounded crests, and unvegetated or *seif* dunes characterized by their sharp crests (Lancaster, 1995; Pye and Tsoar, 2009).

The rounded crest, with straight to slightly sinuous ridges, oriented parallel to the main drift potential direction (RDD) and RDP/DP ratio of the landforms here presented, aligns with the characteristics of moderately to highly deflated linear dunes, suggesting their classification as such. Additionally, the gravelly clastic superficial cover (immature or incipient desert pavement) distribution as a mantle over the entire area, rather than being concentrated on the crests as described in the literature (Milana, 2009; Yizhaq *et al.*, 2009; Gough *et al.*, 2020), and their arrangement as isolated bodies, when wavelength is characteristic of ripples, dismisses the idea of using megarriples to define them.

Under this theoretical framework, it is considered that the occurrence of these linear dunes in the Apocango River terraces could be associated with different stages of eolian aggradation/erosion (Fig. 14), linked to the surrounding topography generated by fluvial action and neotectonic activity. These morphologies follow the pattern of secondary ephemeral fluvial channels, indicating their association with alluvial activity (Hugenholtz *et al.*, 2017). Thus, it could be established that in the first stage, the analyzed area was dominated by the eolian sedimentation of linear dunes associated with the migration of wind ripples. Similar conditions are observed to the west in the proximal to middle Apocango fan, in Campo de Anchoco, where a dune system extends from west to east, comprising active barchans, transverse dunes, and linear dunes with crests-oriented NE-SW (Fig. 13, Ciccioli *et al.*, 2021). Additionally, sand shadows and Zibars occurred in the middle part of the Apocango fan (Ciccioli *et al.*, 2021). In the second stage, erosional processes (deflation) were dominant in the area, preserving only fine sediments (muddy sand) of the linear dunes in protected areas related to probably the margins of small secondary channels or gullies (Fig. 14). In this stage, active deflation led to the rounding of linear dune crests (the analyzed landforms), the formation of poorly developed desert pavements (immature or incipient) covering all the surfaces, and deflation holes (Fig.14). Once the desert pavement was established, it stabilized the linear dunes making it difficult for the wind to transport and remove the coarse grains. This protective layer ensures that the dunes remain immobile. This last stage is currently recognized where given the arid environmental conditions and preferential wind directions from the southwest (SW-WSW), leading to the formation of eolian sand accumulations in the central and northeast (NE) sectors of the valley (*e.g.* Medanitos and Tatón dune fields).

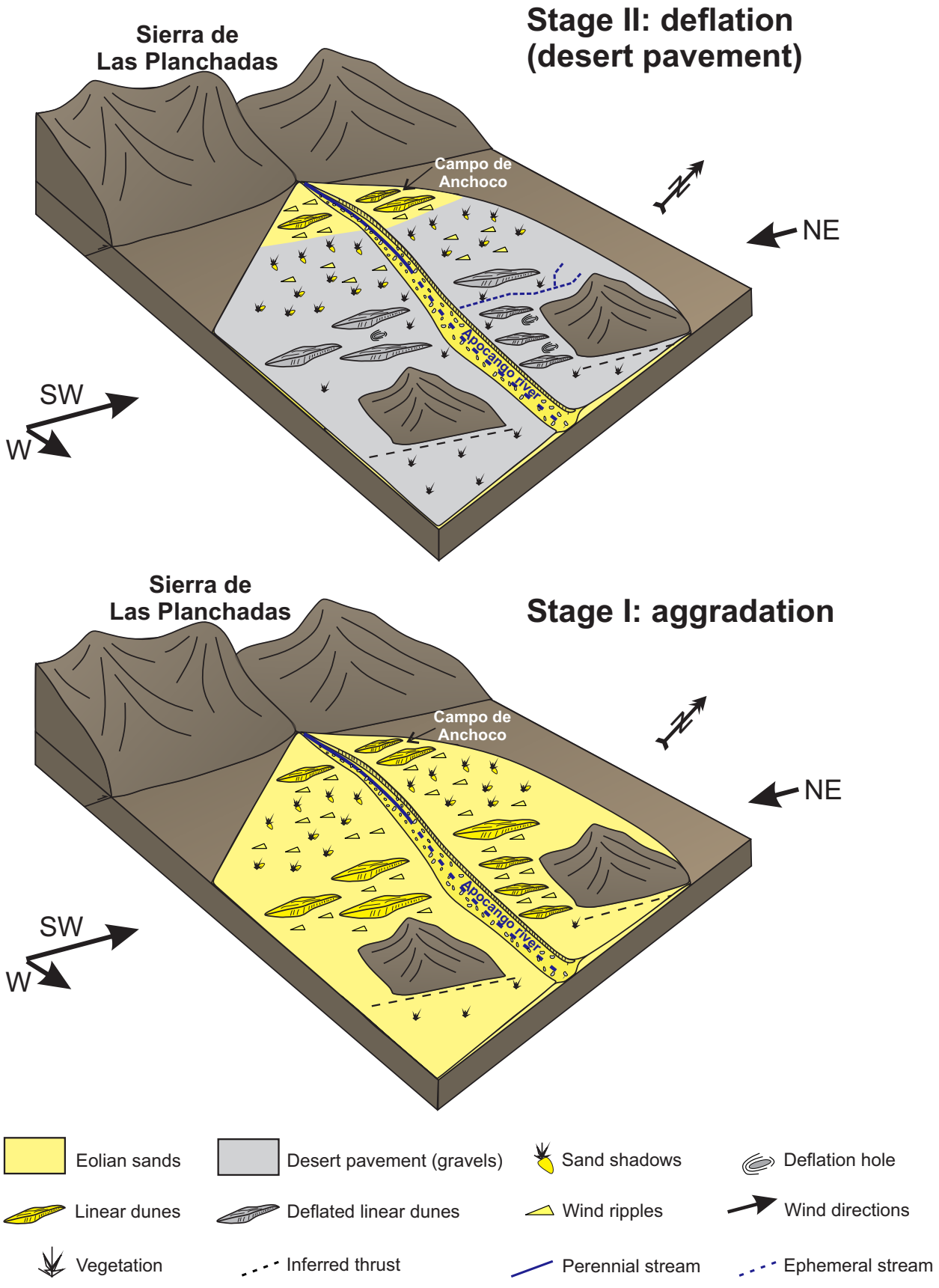

Figure 14. Model of the evolution of the studied area, with the illustration of the first stage dominated by eolian sedimentation and the second stage where deflation prevailed.

CONCLUSIONS

A study of linear landforms found in the valley, specifically in the narrow gorge delimited by Pliocene-Pleistocene pedimented unit (Rodados de la Puna Formation) and ancient piedmont deposit levels on the Apocango River terraces as well as to the west, has been conducted.

The most relevant results are:

1) The linear landforms analyzed exhibit similar characteristics with dunes but remain immobile.

2) They are composed of a bimodal cover of medium to coarse pebble (-4.5 to -3.5 φ) and fine sand (2.5 φ), and beneath this cover, protected by it, is a fine to medium sand (2.66 - 1.31 φ) grain size layer.

3) The sandy gravel superficial cover is interpreted as a poorly evolved desert pavement since, on average, the gravelly fraction (>2 mm) represents between 44.49% and 58.60%. Eolian deflation is considered one of the main contributors to its development.

4) Based on the compositional characteristics obtained, it is interpreted that the primary source of gravelly and sandy material comes from the west (Sistema de Famatina). The sediment is transported by the Apocango River and the wind.

5) It is suggested to define the studied landforms as moderately to highly deflated linear dunes because of their straight to slightly sinuous ridges, rounded crests, parallel orientation to the main drift potential direction (RDD), and RDP/DP ratio.

6) The genesis of these linear dunes is interpreted to be linked to the occurrence of different stages of eolian aggradation/erosion associated with the surrounding topography: Stage I - the predominance of eolian sedimentation of linear dunes associated with the migration of wind ripples; Stage II - development of an immature desert pavement resulting from the prevalence of erosive processes (deflation), which, together with the preservation of fine sediments in protected areas (probably related with margins of small secondary channels and gullies), give rise to immobile linear morphologies with rounded crests.

Acknowledgments. This work was carried out within the framework of the UBACyT ID 2018 Mod I 20620170100007BA, UBACyT 2023 Mod I 20020220100186BA, and PICT 2019-01723 (PC). We appreciate the support from the Department of Geological Sciences at the Universidad de Buenos Aires for field and laboratory activities. We would like to express our special gratitude to Dr. Carlos Oscar Limarino and Dr. Rubén López, who served as advisors for the Undergraduate thesis that forms the basis of this manuscript. Additionally, we extend our thanks to Dr. Norma Ratto and Horacio Tassone for their valuable collaboration in fieldwork. Finally, we wish to acknowledge the insightful comments and suggestions of J.P. Milana and S. Moreiras, which played a crucial role in improving this manuscript.

REFERENCES

Báez, W.A., Chiodi, A.L., Bustos, E., Arnosio, J.M., Viramonte, J.G., Giordano, G., and Alfaro Ortega, B.B. (2017). Mecanismos de emplazamiento y destrucción de los domos lávicos asociados a la caldera del Cerro Blanco, Puna Austral. *Revista de la Asociación Geológica Argentina 74* (2): 227-238.

Bagnold, R. A. (1954). *The physics of blown sand and desert dunes*. Methuen, London, 265 pp.

Blair, T.C. and McPherson, J.G. (1999). Grain-size and textural classification of coarse sedimentary particles. *Journal of Sedimentary Research, 69*(1): 6-19.

Bruniard, E.D. (1982). La diagonal árida argentina: un límite climático real. *Revista Geográfica, 95*: 5-20.

Bullard, J. E. (1997). A note on the use of the" Fryberger method" for evaluating potential sand transport by wind. *Journal of Sedimentary Research, 67*(3), 499-501.

Ciccioli, P.L., Ratto, N.R., Fernandez Molina, D. and Castañeda, M.E. (2021). Miradas interdisciplinarias sobre los procesos ambientales actuantes en la localidad arqueológica de Mishma (Bolsón de Fiambalá, departamento de Tinogasta, Catamarca). *Relaciones, 46*(2): 31-40.

Cox, E.P. (1927). A method of assigning numerical and percentage values to the degree of roundness of sand grains. *Journal of Paleontology, 1*(3): 179-183.

Cooke, R.U. and Warren, A. (1973). *Geomorphology in deserts.* Berkeley: University of California Press. 394 pp.

Cooke, R., Warren, A. and Goudie, A. (1993). *Desert Geomorphology*. UCL Press, London 526 pp.

De Silva, S.L., Spagnuolo, M.G., Bridges, N.T. and Zimbelman, J.R. (2013). Gravel-mantled megaripples of the Argentinean Puna: A model for their origin and growth with implications for Mars. *Geological Society of America Bulletin 125* (11-12): 1912-1929.

Deri, M.N. (2016). *Sedimentología del campo de dunas de Medanitos, Bolsón de Fiambalá, Provincia de Catamarca.* Trabajo Final de Licenciatura, Facultad de Ciencias Exactas y Naturales, Universidad de Buenos aires, 126 pp. (inédita).

Deri, M.N. and Ciccioli, P.L. (2017). *Distintos tipos de óndulas eólicas del Campo de Dunas de Medanitos, Bolsón de Fiambalá, Provincia de Catamarca.* XX Congreso Geológico Argentino: 12-17, San Miguel de Tucumán.

Deri, M.N. and Ciccioli, P.L. (2018). Sedimentología del campo de dunas intermontano de Medanitos, Bolsón de Fiambalá,

Catamarca. *Revista de la Asociación Geológica Argentina 75* (3): 325-345.

Deri, M., Ciccioli, P., Amidon, W. and Marenssi, S. (2019). *Estratigrafía y edad máxima de depositación de la Formación Tambería en el Bolsón de Fiambalá, Catamarca.* 5° Simposio del Mioceno-Pleistoceno del Centro y Norte de Argentina: 53-56, Jujuy.

Dixon, J.C. (2009). Aridic soils, patterned ground, and desert pavements. En: Parson y Abrahams Springer (Eds.) *Geomorphology of desert environments*: 101-122.

Fernandez Molina, D. (2020). *Sedimentología del Zanjón de Apocango, Bolsón de Fiambalá, Catamarca*. Trabajo Final de Licenciatura, Facultad de Ciencias Exactas y Naturales, Universidad de Buenos Aires, 129 pp. (inédito).

Folk, R.L. (1954). The distinction between grain size and mineral composition in sedimentary-rock nomenclature. *The Journal of Geology, 62*(4): 344-359.

Folk, R.L. and Ward W.C. (1957). Brazos River bar: a study in the significance of grainsize parameters. *Journal of Sedimentary Petrology 27*(1): 3-26.

Folk, R.L. Andrews, P.B. and Lewis, D.W. (1970). Detrital sedimentary rock classification and nomenclature for use in New Zealand. *New Zealand Journal of geology and geophysics,13*(4): 937-968.

Fryberger, S.G. (1979). Dune forms and wind regime. In: McKee, E.D. (Ed.), *A Study of Global Sand Seas*, USGS Professional Paper. Vol. 1052. USSG and NASA, Washington, DC,pp. 137-169.

Fryberger, S. G., Hesp, P. and Hastings, K. (1992). Aeolian granule ripple deposits, Namibia. *Sedimentology, 39*(2): 319-331.

Garleff, K., Stingl, H. and Veit, H. (1994). New dates on the Late Quaternary history of landscape and climate in the Bolsón of Fiambalá, NW Argentina (Province Catamarca). *Zentralblatt für Geologie und Paläontologie. Teil 1, Allgemeine, angewandte, regionale und historische Geologie,* (1/2): 333-341.

Garreaud, R.D., Vuille, M., Compagnucci, R. and Marengo, J. (2009). Present-day South American climate. *Palaeogeography, Palaeoclimatology, Palaeoecology* 281 3: 180-195.

Goudie, A.S. (2013). *Arid and semi-arid geomorphology.* Cambridge university press.

Gough, T., Hugenholtz, C. and Barchyn, T. (2020), Eolian megaripple stripes. *Geology, 48*(11): 1067-1071.

Greeley, R. and Iversen, J. D. (1985). *Wind as a geological process: on Earth, Mars, Venus and Titan*: New York. Cambridge Univ. Press.

Grove, A.T. (1977). The geography of semi-arid lands. *Philosophical Transactions of the Royal Society of London. B, Biological Sciences, 278* (962), 457-475.

Havholm, K. G. and Kocurek, G. (1988). A preliminary study of the dynamics of a modern draa, Algodones, southeastern California, USA. *Sedimentology, 35*(4): 649-669.

Hugenholtz, C.H. and Barchyn, T.E. (2017). A terrestrial analog for transverse aeolian ridges (TARs): Environment, morphometry, and recent dynamics. *Icarus*, 289: 239-253.

Hunter, R.E. (1977). Basic types of stratification in small eolian dunes. *Sedimentology, 24*(3): 361-387

Isla, F. and Espinosa, M. (2017). Upper quaternary evolution of the dune field of the Bolsón de Fiambalá, Catamarca: Sand dispersal at the Andes piedmonts. *Quaternary International* 442: 59-66.

Isla, F.I., Isla, M.F., Bértola, G.R., Bedmar, J.M., Cortizo, L.C. and Maenza, R.A. (2021). Taton dune field: wind selection across the Southamerican arid diagonal, Puna Argentina. *Quaternary and Environmental Geosciences,12*(2):19-29.

Lämmel, M., Meiwald, A., Yizhaq, H., Tsoar, H., Katra, I. and Kroy, K. (2018). Aeolian sand sorting and megaripple formation. *Nature Physics, 14*(7): 759-765.

Lancaster, N. (1995). *Geomorphology of Desert Dunes*. Routledge, London.

Mabbutt, J.A. (1965). Stone distribution in a stony tableland soil. *Australian Journal of Soil Research* 3: 131-142.

Mabbutt, J.A. (1977). *Desert landforms*. Australian National University Press.

McKee, E.D. (1979). *A study of global sand seas.* (Vol. 1052). US Government Printing Office.

Medina, C. (2015). *Petrophysical Study of Reservoir Rocks: Use of Image Analysis Software (IAS) and Mercury Injection Capillary Pressure (MICP) Data*. https://www.slideshare.net/CristianMedina14/petrophysical-study-of-reservoir-rocks-use-of-image-analysis-software-ias-and-mercury-injection-capillary-pressure-micp-data

Meigs, P. (1953). World distribution of arid and semi-arid homoclimates, in Review of research on Arid Zone Hydrology. *Arid zone program*, 1, 203-209.

Milana, J.P. (2009). Largest wind ripples on Earth? *Geology, 37* (4): 343-346.

Montero López, M.C., Hongn, F., Affonso Brod, J., Seggiaro, R., Marrett, R. and Sudo, M. (2010). Magmatismo ácido del mioceno superior-cuaternario en el área de Cerro Blanco-La Hoyada, Puna Austral. *Revista de la Asociación Geológica Argentina, 67*(3): 329-348.

Montero López, M.C., Guzman, S.R. and Hongn, F.D. (2011). Ignimbritas de la quebrada del río Las Papas (Cordillera de San Buenaventura, Catamarca): una primera aproximación petrológica y geoquímica. *Acta geológica, 23*(1-2):78-93.

Munsell Color (Firm). (2009). *Munsell Soil Color Charts: with genuine Munsell color chips*. Grand Rapids, MI: Munsell Color.

Nielson, J. and Kocurek, G. (1986). Climbíng zibars of the Algodones. Sedimentary *Geology 48*(1-2): 1-15.

Pettijohn, F.J., Potter, P.E. and Siever, R. (1987). *Sand and sandstone*. Springer- Verlag, New York, 521pp.

Powers, M.C. (1953) A new roundness scale for sedimentary particles. *Journal of Sedimentary Research, 23* (2), 117-119.

Pye, K. and Tsoar, H. (2009). Aeolian bed forms. *Aeolian sand and sand dunes*, 175-253.

Quiroga, R., Peña, M., Poblete, F., Giambiagi, L., Mescua, J., Gómez, I., Echaurren, A., Perroud, S., Suriano, J., Martínez F. and Espinoza, D. (2021). Spatio-temporal variation of the strain field in the southern Central Andes broken-foreland (27° 30 S) during the Late Cenozoic. *Journal of South American Earth Sciences, 106*: 102981.

Ramos, V.A. (1999). Las provincias geológicas del territorio argentino. *Geología Argentina, Instituto de Geología y Recursos Minerales, Buenos Aires, 29*(3): 41-96.

Ramos, V.A., Cristallini, E.O. and Pérez, D.J. (2002). The Pampean Flat-Slab of the Central Andes. *Journal of South American Earth Sciences, 15*(1): 59-78.

Ratto, N., Montero, C. and Hongn, F. (2013). Environmental instability in western Tinogasta (Catamarca) during the Mid-Holocene and its relation to the regional cultural development. *Quaternary International, 307*: 58-65.

Retallack, G.J. (2001). *Soils of the Past*, second ed. Blackwell Science Ltd., Oxford, p. 404.

Rubiolo, R., Martinez, L. and Pereyra, F. (2003). *Fiambalá 2769-IV, Provincias de Catamarca y Jujuy.* Instituto de Geología y Recursos Minerales, Servicio Geológico Minero Argentino, Buenos Aire, Boletín, 421, 77pp.

Scasso, R.A. and Limarino, C.O. (1997). P*etrología y diagénesis de rocas clásticas.* Asociación Argentina de Sedimentología, Buenos aires, 258 pp.

Sharp, R. P. (1963). Wind ripples. *The Journal of Geology, 71*(5): 617-636.

Sneed, E.D. and Folk, R.L. (1958). Pebbles in the lower Colorado River, Texas a study in particle morphogenesis. J*ournal of Geology, 66(2*): 114-150.

Taira, A. and Scholle, P. A. (1979). Discrimination of depositional environment using settling tube data. J*ournal of Sedimentary Petrology 49(*3): 787-800.

Viera, V. (1982). *Geomorfología (control de médanos). Área: Fiambalá (provincia de Catamarca).* Proyecto NOA hídrico segunda Fase. Consejo Federal de Inversiones, Buenos Aires, 44 pp. (inédito).

Wilson, I. G. (1972). Aeolian bedforms -their development and origins. *Sedimentology, 19(*3-4): 173-210.

Yizhaq, H., Isenberg, O., Wenkart, R., Tsoar, H. and Karnieli, A. (2009). Morphology and dynamics of aeolian mega-ripples in Nahal Kasuy, southern Israel. *Israel Journal of Earth Sciences,* 57: 149-165.

Yizhaq, H. and Katra, I. (2015). Longevity of aeolian megaripples. *Earth and Planetary Science Letters*, 422: 28-32.

Zimbelman, J. R., Williams, S. H. and Johnston, A. K. (2012). Cross-sectional profiles of sand ripples, megaripples, and dunes: a method for discriminating between formational mechanisms. *Earth Surface Processes and Landforms*, 37(10): 1120-1125.